Universitat Autònoma de Barcelona

Self-assembly of functional chromophores into chiral nanomaterials

Cristina Oliveras González

Tesi doctoral

Doctorat de Ciència dels Materials

Director/a	Co-director/a	Tutor/a
David B. Amabilino	Núria Aliaga Alcalde	Jordi Hernando Campos

Departament de Química

Facultat de Ciències

2015

Chapter 3

Bottom-up approach to C_3 symmetric chiral aggregates

3. Bottom-up approach to C_3 symmetric chiral aggregates.

3.1. Introduction.

Organic π-conjugated molecules with columnar organization driven by a co-facial stacked aromatic cores and surrounded by alkyl chains offers great possibilities toward the creation of nanomaterials applicable in energy or charge transport in organic electronic devices such as solar cells or organic field-effect transistor (OFETs).[1,2]

Different rotational symmetries have been studied for discotic molecules, but the C_3 symmetrical structures have become the most attractive,[3,4] especially those ones with 1,3,5-benzenetricarboxamide unit as a central core.[5] These molecules are made by a central core linked to three conjugated identical arms with electronic and optical properties that can be modified by the supramolecular organization and its morphology at the nano- and mesoscale.[6]

The peripheral substitution can be directly covalent linked to the central aromatic-amide platform[7] or can be connected to a spacer that at the same time is covalent bonded to the central core through the amide group (Figure 1).[8]

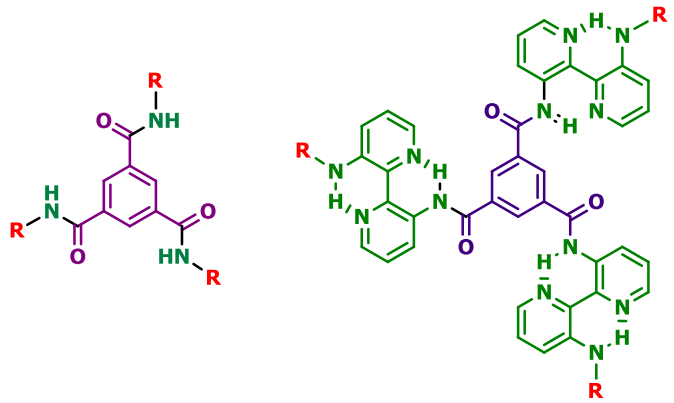

Figure 1. C_3 symmetrical structures based on 1,3,5-benzenecarboxamide.

A common spacer is the 3,3'-diamino-2,2'-bipyridine, that can control the self-assembly process of the molecule. The intramolecular hydrogen-bonding among this unit can rigidify the central core

(1) Sergeyev, S.; Pisula, W.; Geerts, Y. H. *Chem. Soc. Rev.* **2007**, *36*, 1902-1929.
(2) Beltrán, E.; Serrano, J. L.; Sierra, T.; Giménez, R. *J. Mater. Chem.* **2012**, *22*, 7797-7805.
(3) Shu, W.; Valiyaveettil, S. *Chem. Commun.* **2002**, 1350-1351.
(4) Boden, N.; Bushby, R. J.; Hardy, C.; Sixl, F. *Chem. Phys. Lett.* **1986**, *123*, 359-364.
(5) van Gorp, J. J.; Vekemans, J. A. J. M.; Meijer, E. W. *J. Am. Chem. Soc.* **2002**, *124*, 14759-14769.
(6) Kanibolotsky, A. L.; Perepichka, I. F.; Skabara, P. J. *Chem. Soc. Rev.* **2010**, *39*, 2695-2728.
(7) Dai, Y.; Zhao, X.; Su, X.; Li, G.; Zhang, A. *Macromol. Rapid Commun.* **2014**, *35*, 1326-1331.
(8) Danila, I.; Pop, F.; Escudero, C.; Feldborg, L. N.; Puigmartí-Luís, J.; Riobé, F.; Avarvari, N.; Amabilino, D. B. *Chem. Commun.* **2012**, *48*, 4552-4554.

favoring a secondary structure driven by π-π stacking between the 3,3'-diamino-2,2'-bipyridine moiety. This central organization can lead helical columnar supramolecular architectures of the chiral C_3 symmetric molecule (Figure 1).[9,10]

It exists a broad variety of C_3 symmetric molecules and a well-studied C_3 symmetric family based on the 1,3,5-benzenecarboxamide core bonded to 3,3'-diamino-2,2'-bipyridine. The possibility to modify systematically the peripheral arms offers a great number of derivatives that easily tune their physical properties in order to be integrated in nanoelectronics[11] or optical devices.[12] Moreover, the introduction of chiral centers in the arms can influence the charge transport in the chiral aggregates.[13]

3.2. Objectives

The objective of this project is:

The bottom-up approach to chiral nanofibers suitable for charge transport processes.

The project will therefore center in the following concrete objectives:

- Prepare chiral functional molecules derived from porphyrins with different twist between the units and determine the efficiency of the transport in these systems.
- Determine the influence of the position of the stereogenic center and molecular constitution on the hierarchical transfer of chirality into material morphology.

C_3 symmetric discotic molecules C_3-(*R,R,R*)-**1** and C_3-(*R,R,R*)-**2** have been designed and synthetized to probe the influence of the molecular constitution in the hierarchy organization (Figure 2).

(9) Palmans, A. R. A.; Vekemans, J. A. J. M.; Meijer, E. W. *Recl. Trav. Chim. Pays-Bas.* **1995**, *114*, 277-284.
(10) Palmans, A. R. A.; Vekemans, J. A. J. M.; Fischer, H.; Hikmet, R. A.; Meijer, E. W. *Chem. Eur. J.* **1997**, *3*, 300-307.
(11) van Herrikhuyzen, J.; Jonkheijm, P.; Schenning, A. P. H. J.; Meijer, E. W. *Org. Biomol. Chem.* **2006**, 4, 1539-1545.
(12) van Hameren, R.; Schön, P.; van Buul, A. M.; Hoogboom, J.; Lazarenko, S. V.; Gerritsen, J. W.; Engelkamp, H.; Christianen, P. C. M.; Heus, H. A.; Maan, J. C.; Rasing, T.; Speller, S.; Rowan, A. E.; Elemans, J. A. A. W.; Nolte, R. J. M. *Science* **2006**, *314*, 1433-1436.
(13) Danila, I.; Riobé, F.; Piron, F.; Puigmartí-Luís, J.; Wallis, J. D.; Linares, M.; Agren, H.; Beljone, D.; Amabilino, D. B.; Avarvari, N. *J. Am. Chem. Soc.* **2011**, *133*, 8344-8353.

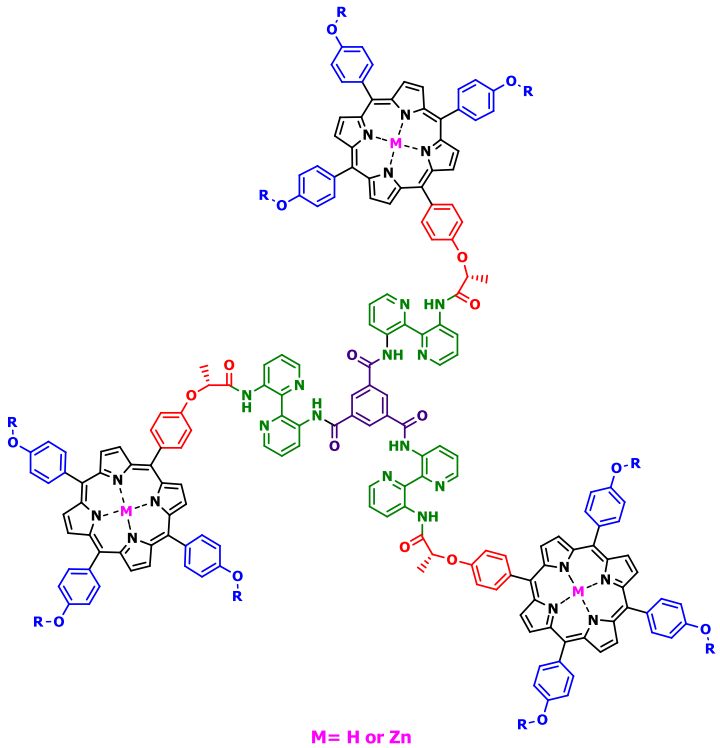

Figure 2. Target C_3 discotic molecules.

The compounds differ on the number of carbons of the alkyl chains in the surrounding of the porphyrin ring, that could influence the self-assembly of the symmetric discotic molecules. Moreover, the introduction of a metal such as the zinc (II) ion in the core of the chromophore might affect the morphology of the nanomaterial as well as its optical and electrical properties.[14]

In this work, the targeted compounds have been studied in solution by circular dichroism spectroscopy (CD) to determine their hierarchical organization,[15] while the morphology of the aggregates was investigated by atomic force microscopy (AFM) after their transfer from solution to the studied surfaces.[16] For this purpose, different solvents were used to investigate the influence of the polarity of the solvent on the supramolecular organization of the C_3-molecules.[17]

(14) Singh, D. K.; Nath, M. *Dyes Pigments* **2015**, *121*, 256-264.
(15) Pescitelli, G.; Gabriel, S.; Wang, Y.; Fleisschhauer, J.; Woody, R. W.; Berova, N. *J. Am. Chem. Soc.* **2003**, *125*, 7613-7628.
(16) Jonkheijm, P.; Hoeben, F. J. M.; Kleppinger, R.; Van Herrikhuyzen, J.; Schenning, A. P. H. J.; Meijer, E. W. *J. Am. Chem. Soc.* **2003**, *125*, 15941-15949.
(17) van Hameren, R.; van Buul, A. M.; Castriciano, M. A.; Villari, V.; Micali, N.; Schon, P.; Speller, S.; Scolaro, L. M.; Rowan, A. E.; Elemans, J. A. A. W.; Nolte, R. J. M. *Nano Lett.* **2008**, *8*, 253-259.

3.3. Synthesis of chiral C_3 discotic molecules.

C_3 symmetric discotic molecules based on chiral porphyrins have been synthesized following the synthetic route showed in Scheme 1.

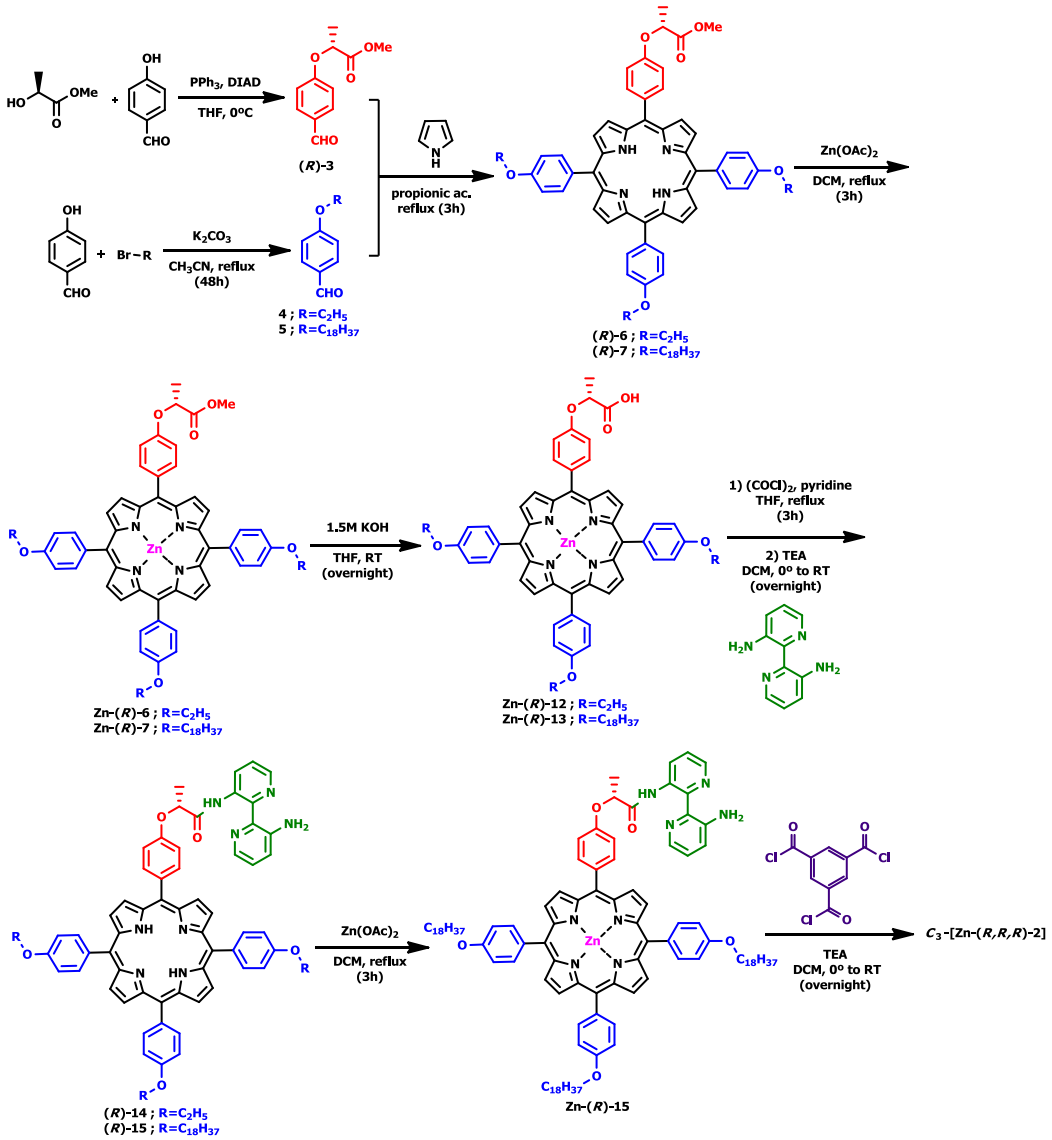

Scheme 1. Synthesis of the C_3-discotic molecule.

3.3.1. Synthesis of the chiral aldehyde (*R*)-3 by Mitsunobu reaction.

The chiral aldehyde derivative of the lactate group was prepared by a Mitsunobu reaction (Scheme 2).[18]

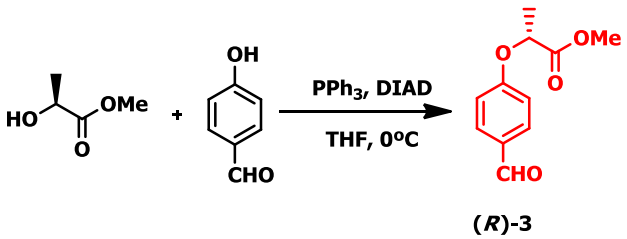

(*R*)-3

Scheme 2. Synthesis of lactate aldehyde (*R*)-**3** by Mitsunobu reaction.

The lactate benzaldehyde (*R*)-**3** was achieved by the reaction between the commercially available compounds 4-hydroxy-benzaldehyde and (*S*)-(-)-Methyl lactate in dry conditions, using triphenylphosphine and diisopropyl-azodicarboxylate as reagents.[19]

3.3.2. Synthesis of the alkoxyaldehydes 4 and 5.

The alkoxybenzaldehyde derivatives **4** and **5** are obtained after a Williamson reaction between the commercially available 4-hydroxy-benzaldehyde and the corresponding bromoalkyl in basic conditions (Scheme 3).[20]

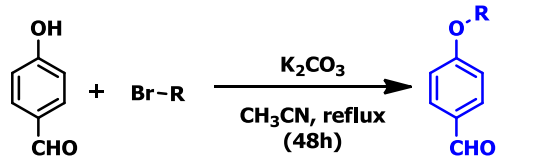

4 ; R=C_2H_5
5 ; R=$C_{18}H_{37}$

Scheme 3. Synthesis of the alkoxyaldehydes **4** and **5**.

The Williamson reaction is a typical nucleophilic substitution (S_N2) developed in 1980s by Alexander Williamson. The general mechanism is the nucleophilic attack of the alkoxy group to the bromoalkyl derivative (Scheme 4).

(18) Minguet, M.; Amabilino, D. B.; Vidal-Gancedo, J.; Wurst, K.; Veciana, J. *J. Mater. Chem.* **2002**, *12*, 570-578.
(19) This step has been explained in detail in **Chapter 2**.
(20) Eleftheriadis, N.; Thee, F.; te Biesebeek, J.; van der Wouden, P.; Baas, B.-J.; Dekker, F.J. *Eur. J. Med. Chem.* **2015**, *94*, 265-275.

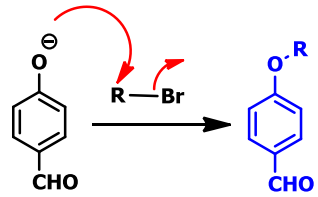

Scheme 4. Mechanism of the Williamson reaction.

One should notices that in this reaction the alkoxy group acts as a nucleophile instead of the alcohol, as the alkoxy group is more reactive than the alcohol. For this reason, the reaction was performed in basic conditions, in order to generate the alkoxy-benzaldehyde during the reaction process.

3.3.3. Formation of the porphyrin ring.

The goal of this work was to synthesize C_3 symmetric molecules based on chiral porphyrins that contain in their structure the chiral group resulting from de lactate benzaldehyde derivative (*R*)-**3** and the corresponding alkoxybenzaldehyde in a ratio 1:3.

For this purpose two different methods have been tested.

3.3.3.1. Synthesis of the chiral porphyrin by Adler and Longo method.[21]

The chiral porphyrin derivative was afforded by the condensation of the two aldehydes with pyrrole in refluxing propionic acid (Scheme 5).[22]

(21) Adler, A. D.; Shergali, W.; Longo, F. R. *J. Am. Chem. Soc.* **1964**, *86*, 3145-3149.
(22) The synthesis of porphyrins has been explained in more detail in the general introduction (**Chapter 1**).

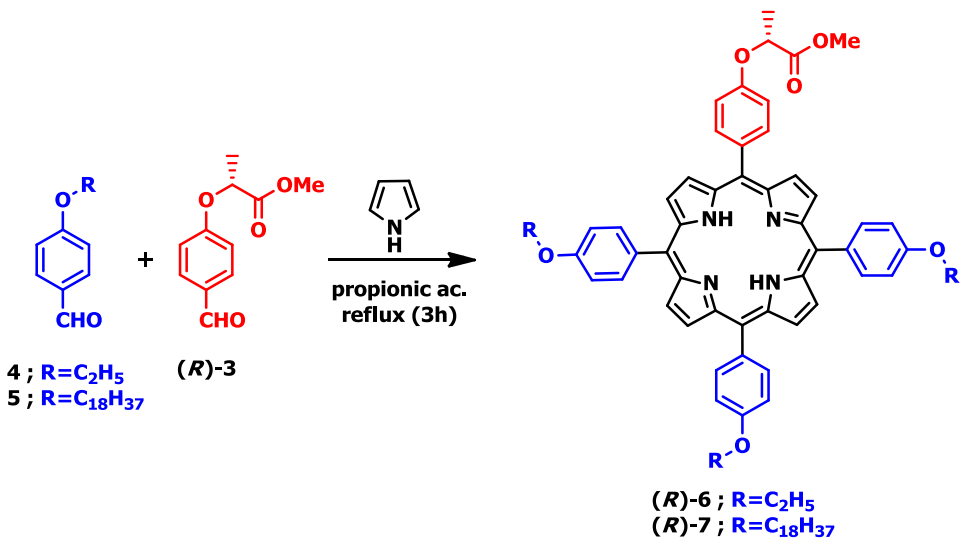

Scheme 5. Synthesis of the porphyrin derivative (*R*)-**6** and (*R*)-**7.**

It is necessary to stand out that, in the reaction process, the achiral symmetric porphyrin was also formed due to the combinatorial chemistry character of the reaction, affording a mixture of porphyrins. Furthermore, additional possible porphyrins were not formed because the molar ratio used in the synthesis (Figure 3).

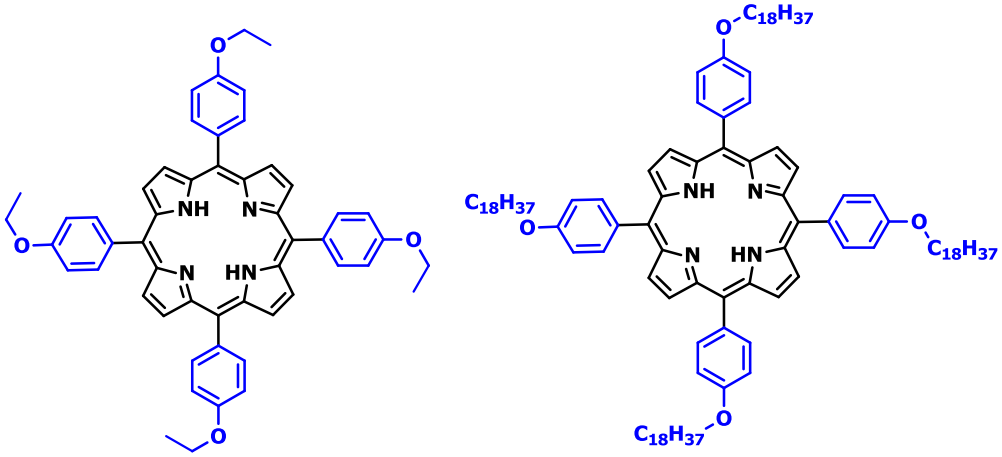

Figure 3. Symmetric achiral porphyrins **8** and **9** obtained in the reaction.

Figure 4 shows the comparison of the ^{1}H-NMR in *d*-chloroform of the chiral porphyrin and the achiral symmetric porphyrin.

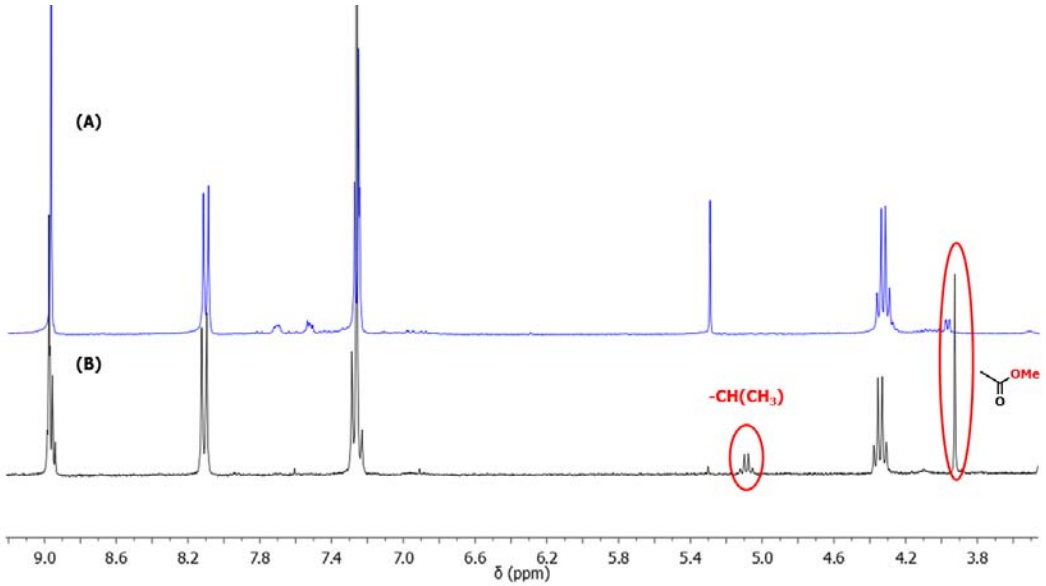

Figure 4. ^{1}H-NMR of the achiral symmetric porphyrin (A) and of the desired chiral porphyrin (B).

As it can be observed in the ^{1}H-NMR spectra, it is easy to recognize the achiral symmetric porphyrin because of the lack of the "chiral" proton at around 5.00 ppm and of the protons related to the ester group at around 3.80 ppm.

3.3.3.2. Synthesis of the chiral porphyrin via dipyrromethane derivatives.

3.3.3.2.1. Synthesis of the dipyrromethane derivative.

Lindsey developed a method to synthesize the dipyrromethane derivative by the condensation of an aldehyde and an excess of pyrrole in presence of a catalyst in a solvent free conditions (Scheme 6).[23]

(23) Lindsey, J. S. *Scalable synthesis of dipyrromethanes*, **2005**, US 2005/0038262 A1.

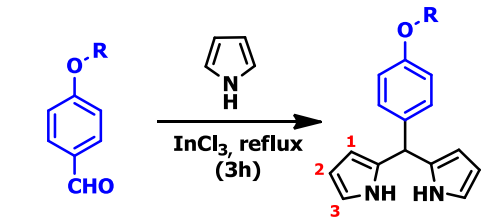

Scheme 6. Synthesis of dipyrromethane 10 and 11.

The crude dipyrromethane derivative was diluted in EtOAc and extracted with H_2O in order to remove the catalyst and the excess of pyrrole. While the dipyrroetoxybenzene derivative **10** was obtain in a 50.2% yield as a brown oil after evaporation of the solvent, the dipyrrol derivative **11** was obtain in a 45.8% yield after crystallization in methanol as a pale yellow-white solid.

Figure 5 shows the ^{1}H-NMR of any of the two dipyrromethane derivatives, because the only difference between them is the length of the alkyl chain.

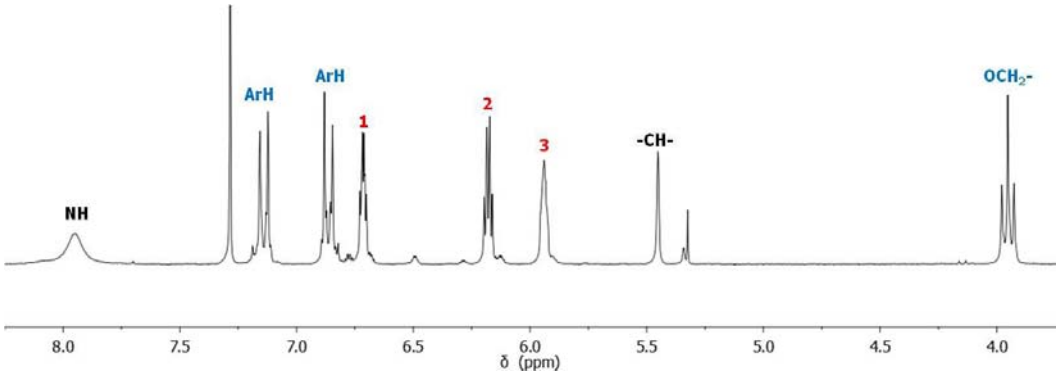

Figure 5. ^{1}H-NMR of the dipyrromethane derivative in *d*-chloroform.

3.3.3.2.2. Synthesis of the chiral porphyrin (*R*)-7.

Typically dipyrromethanes were used for the preparation of *β*–substituted porphyrins, but recently, in the last decade, the use of these intermediates are also used to obtain MacDonald-type [2+2] *meso*-substituted porphyrins,[24] such as the ones studied in this work.

(24) Arsenault, G. P.; Bullock, E.; MacDonald, S. F. *J. Am. Chem. Soc.* **1960**, *82*, 4384-4389.

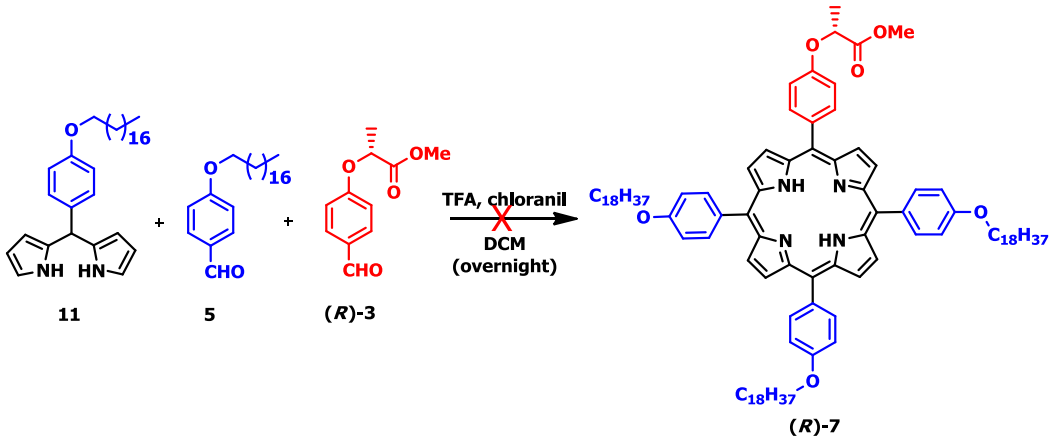

Scheme 7. Synthesis of the chiral porphyrin (*R*)-**7**.

The condensation of a stoichiometric mixture 1:1:1 of the dipyrromethane **11**, octadecaneoxybenzaldehyde **5** and the chiral aldehydes (*R*)-**3** to obtain the desired porphyrin was performed using the Lindsey method.[25,26] For this process mild conditions were used in order to avoid scrambling and obtain the porphyrin in better yields. However, the final compound was not possible to isolate in good amounts after filtration through celite® and several silica gel column chromatography. Therefore this pathways was abandoned and Adler and Longo's method was used.

3.3.4. Metallation of the free-base porphyrin (*R*)-6 and (*R*)-7.

The metallation of the free-base porphyrins was performed in CH_2Cl_2 under argon atmosphere using zinc (II) acetate as a metal salt (Scheme 8).[27]

The crude metalloporphyrin was treated with an aqueous base solution in order to neutralize the acetic acid formed in the process and purified by a short silica gel column chromatography affording approximately 75 % yield as a purple powder for both metalloporphyrins, respectively.

(25) Littler, B. J.; Ciringh, Y.; Lindsey, J. S. *J. Org. Chem.* **1999**, *64*, 2864-2872.
(26) Nowak-Król, A.; Plamont, R.; Canard, G.; Edzang, J. A.; Gryko, D. T.; Balban, T. S. *Chem. Eur. J.* **2015**, *21*, 1488-1498.
(27) Feldborg, L. N.; Saletra, W. J.; Iavicoli, P.; Amabilino, D. B. *J. Porphyr. Phthalocya.* **2011**, *15*, 995-1003.

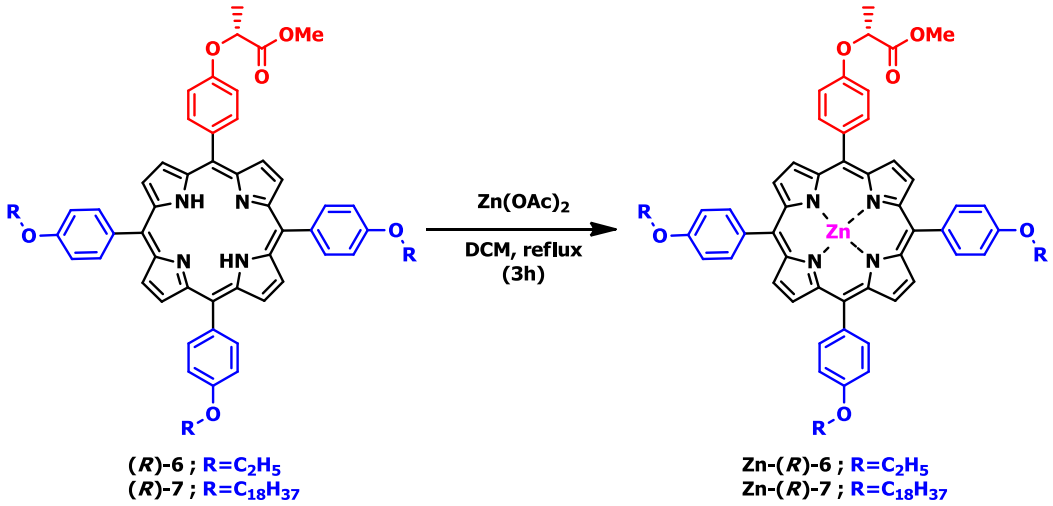

Scheme 8. Synthesis of the metalloporphyrins Zn-(*R*)-**6** and Zn-(*R*)-**7**.

A fast way to identify that the metal ion has been incorporated into the porphyrin ring is by comparison of the absorption UV-Visible spectra. The free-base porphyrins always presents four Q-bands from 500 to 700 nm, whereas for metalloporphyrins only two Q-bands or less are appreciable in the spectrum due to their higher orbital degeneracy because of the symmetry in the structure (**¡Error! No se encuentra el origen de la referencia.**).[28]

Figure 6. Absorption UV-Visible spectra of free-base porphyrin (*R*)-**7** and its metalloporphyrin Zn-(*R*)-**7**.

(28) Gouterman, M. *J. Mol. Spectros.* **1961**, *6*, 138-163.

3.3.5. Synthesis of the chiral acid metalloporphyrins Zn-(*R*)-12 and Zn-(*R*)-13.

The desired C_3 symmetric discotic molecules do not necessarily have a metal ion coordinated in the core of the porphyrin ring. However, the introduction of a zinc metal ion in the chromophoric ring was helpful for the conversion from the ester group to the acid which was easily removed from the aqueous solution.

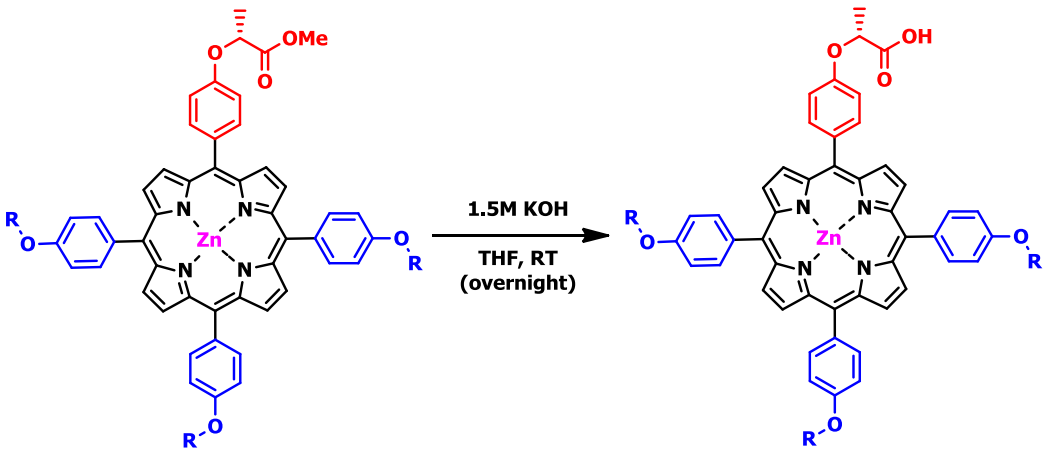

Zn-(*R*)-6 ; R=C_2H_5
Zn-(*R*)-7 ; R=$C_{18}H_{37}$

Zn-(*R*)-12 ; R=C_2H_5
Zn-(*R*)-13 ; R=$C_{18}H_{37}$

Scheme 9. Synthesis of the acid metalloporphyrins Zn-(*R*)-**12** and Zn-(*R*)-**13**.

The saponification reaction of the metalloporphyrins Zn-(*R*)-**6** and Zn-(*R*)-**7** was performed in a THF/1.5M KOH (3:1 v/v) in ambient conditions, affording the desired acids in a good yield, after dissolution in a chlorinated solvent and washed with acidic aqueous solution.

Is worthy to mention that metalloporphyrin Zn-(*R*)-**12** presents low solubility in many solvents, even dichloromethane and chloroform, therefore the study of this compound by ^{1}H-NMR was performed in THF-d_8, solvent in which it is totally soluble.

3.3.6. Coupling between the chiral porphyrin and 3,3'-diamino-2,2'-bipyridine.

The coupling between the chiral porphyrin and the diamino-bipyridine is performed in a two-step reaction, where an acid chloride intermediate, formed in the first step, reacted later with the diamino-bipyridine forming the monoacylated compound (*R*)-**14** and (*R*)-**15** (Scheme 10).[29,30]

(29) Heuzé, K.; Fourmigué, M.; Batail, P. *J. Mater. Chem.* **1999**, *9*, 2373-2379.
(30) Rice, C. R.; Onions, S.; Vidal, N.; Wallis, J. D.; Senna, M.-C.; Pilkington, M.; Stoeckli-Evans, H. *Eur. J. Inorg. Chem.* 2002, 1985-1997.

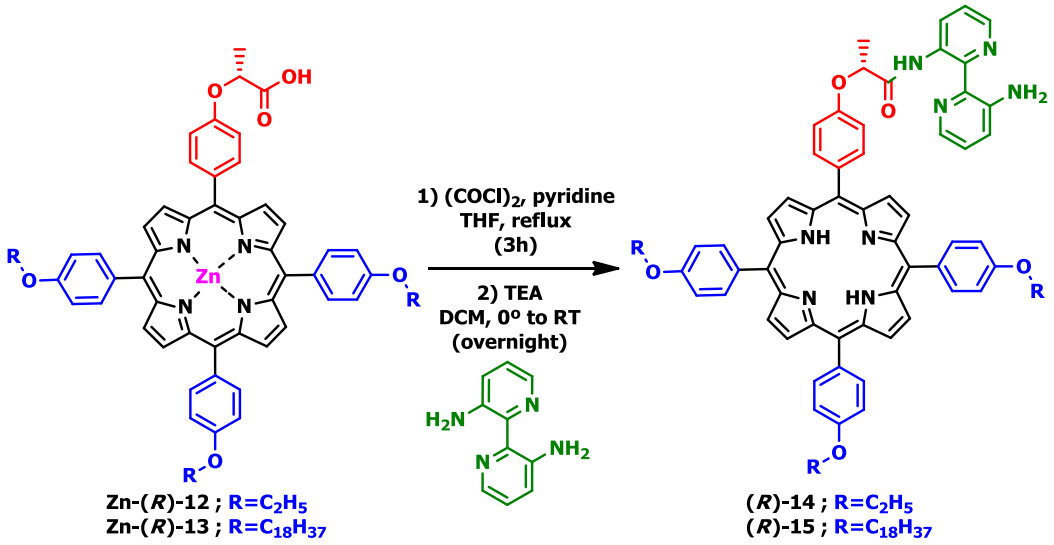

Scheme 10. Synthesis of the monoacylated compound (*R*)-**14** and (*R*)-**15**.

It is important to mention that, during the reaction process, the zinc (II) metal ion jumped out from the porphyrin ring. This happens during the formation of the acid chloride porphyrin intermediate, where the media became too acidic for the pH stability of the zinc (II) metal ion.[31]

Dry conditions were mandatory during all the coupling process and during the addition of bipyridine the control of the temperature was carefully taken into account as another key factor to avoid the formation of side products. Even so, the coupling of two units of chiral porphyrin to the diamino-bipyridine was observed, and the diacylated compounds (*R,R*)-**16** and (*R,R*)-**17** were obtained as minor products (Figure 7).

(31) Hambright, P.; Fleischer, E. B. *Inorg. Chem.* **1970**, *9*, 1757-1761.

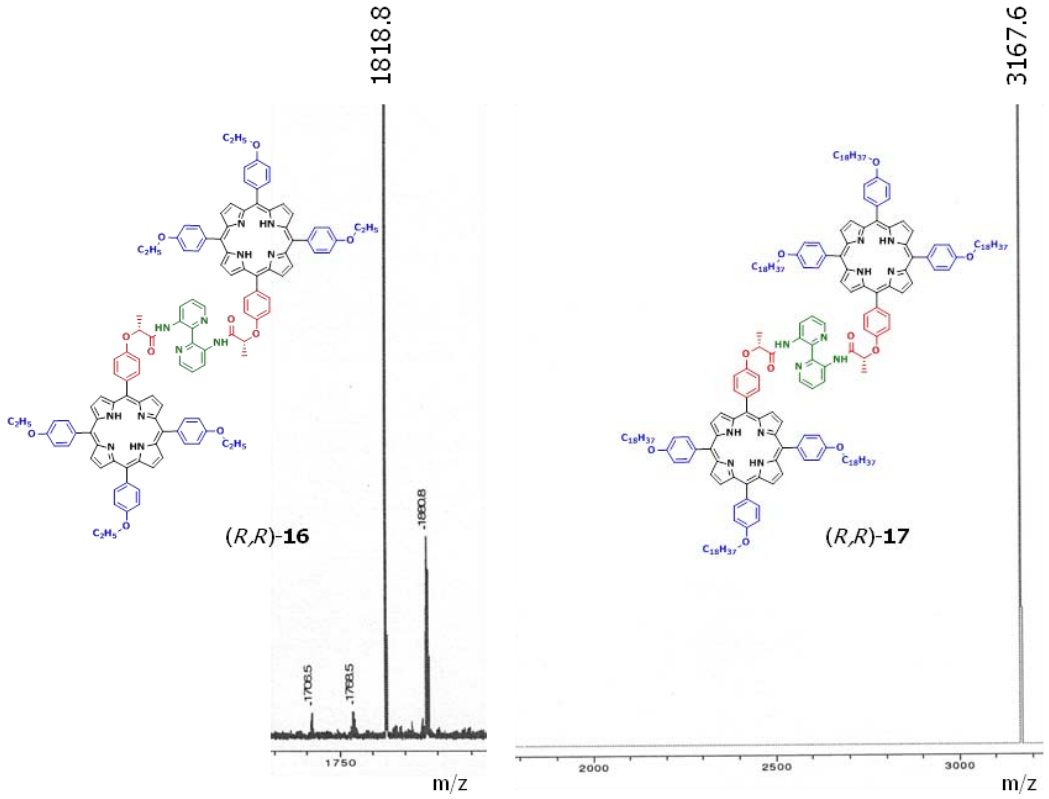

Figure 7. MALDI-Tof spectra of the diacylated compounds (*R,R*)-**16** and (*R,R*)-**17**.

3.3.7. Metallation of the chiral porphyrin-amido-amino-bipyridine (*R*)-15.

The Zn-[porphyrin-amido-amino-bipyridine] was obtained as explained above, by reacting the free-base porphyrin compound with the zinc (II) metallic salt (Scheme 11).

The metallocompound monoacylated derivative was obtained after purification in a 63.5% yield as a purple powder.

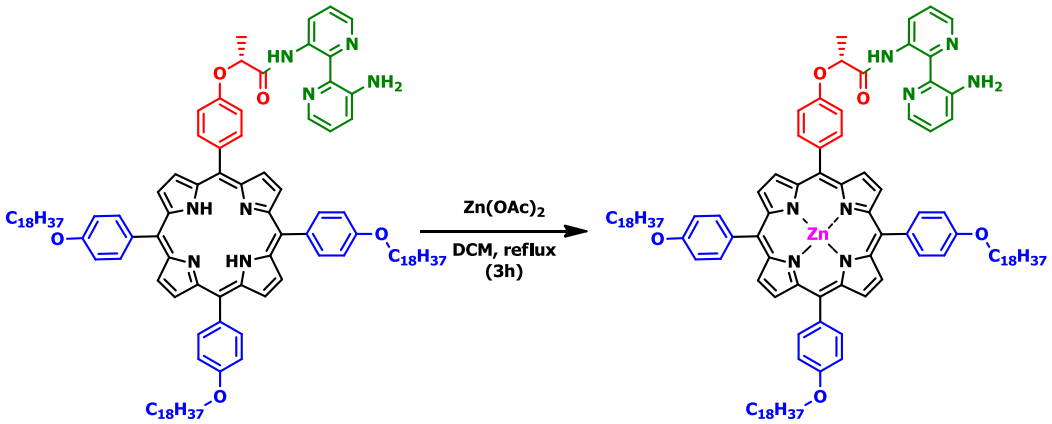

Scheme 11. Synthesis of the Zn-[porphyrin-amido-amino-bipyridine] Zn-(*R*)-**15**.

3.3.8. Synthesis of the C_3 symmetric tris-metalloporphyrin C_3-[Zn-(*R,R,R*)-2].

The final step is the tris-acylation reaction between the trimesic acid chloride and the metalloporphyrin Zn-(*R*)-**15** (Scheme 12).[32]

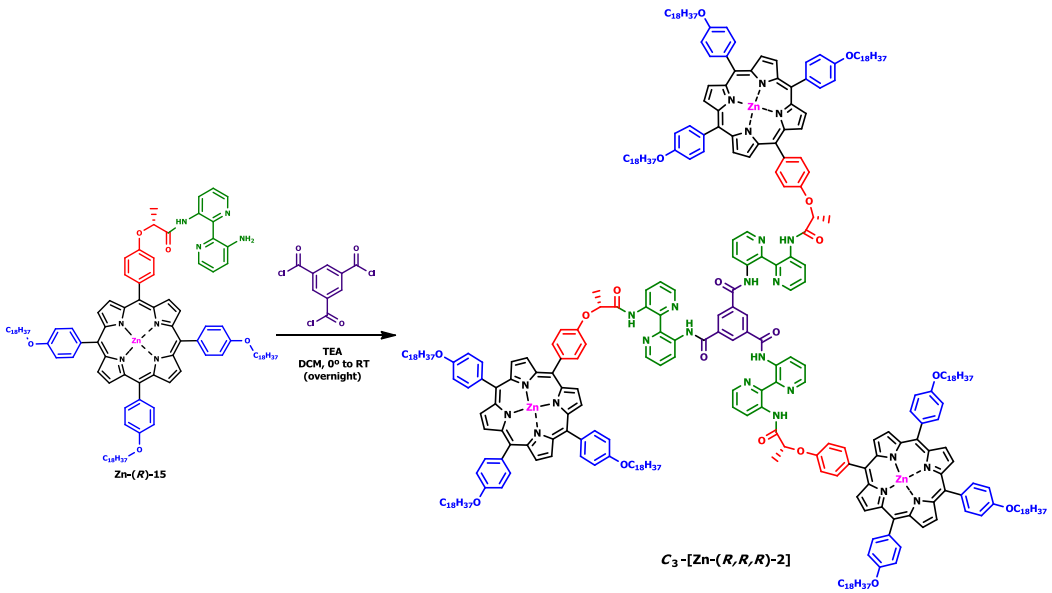

Scheme 12. Synthesis of the final C_3 symmetric tris-metalloporphyrin C_3-[Zn-(*R,R,R*)-**2**].

(32) Danila, I.; Riobé, F.; Puigmarti-Luis, J.; Pérez del Pino, Á.; Wallis, J. D.; Amabilino, D. B.; Avarvari, N. *J. Mater. Chem.* **2009**, *19*, 4495-4504.

The reaction was kept under dry conditions from 0ºC to room temperature overnight. Afterwards, the precipitate formed in the reaction was washed with methanol and ether to obtain a purple powder as a pure compound.

^{1}H-NMR identification for the C_3 symmetric compound was challenging, due to the similarities between the spectra from the starting metalloporphyrin acylated compound and the final one. However, the mass spectrum revealed the formation of the desired final compound (Figure 8).

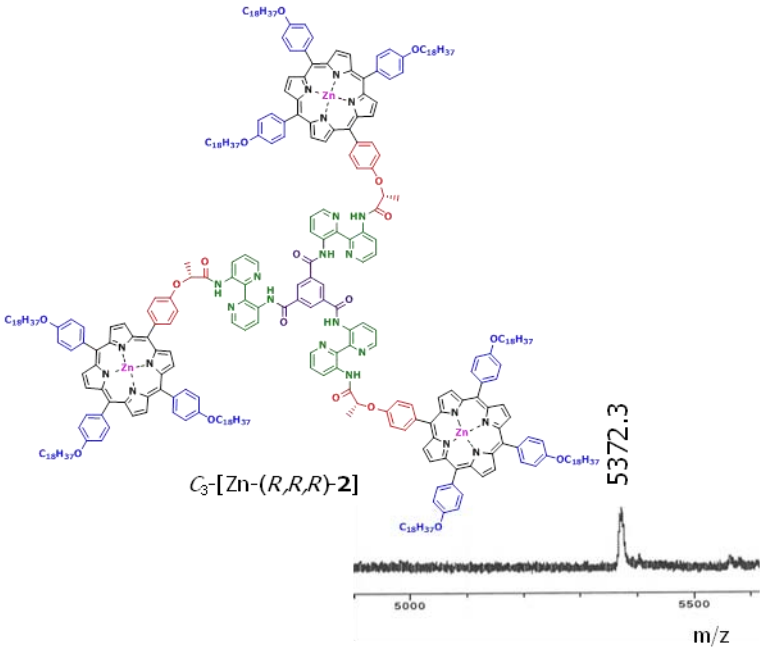

Figure 8. MALDI-Tof spectrum of C_3-[Zn-(*R,R,R*)-**2**].

3.4. Study the self-assembly of C_3-[Zn-(*R,R,R*)-2] by circular dichroism.

Circular dichroism (CD) is an important tool for the self-assembly studies of chiral chromophores due to its sensitivity to the supramolecular structure and absolute configuration.[33]

The chiral C_3 symmetric discotic molecules herein designed can self-assemble through different non-covalent interactions that involve the different groups of the compound. Indeed, the bipyridine moieties rigidify around the central core in a propeller-like conformation drives the self-assembly of the C_3 molecule. In addition, the π-π stacking interactions directly related with the porphyrin skeleton can promote the helical organization of the supramolecular stack, while the peripheral alkyl chains may also influence the supramolecular arrangement of the C_3 compound.

(33) Berova, N.; Di Bari, L.; Pescitelli, G. *Chem. Soc. Rev.* **2007**, *36*, 914–931.

Usually, the non-covalent interactions involved in the hierarchy self-assembly and its strength depends on the nature of the solvent used.[34]

The self-assembly studies of the C_3-[Zn-(*R,R,R*)-**2**] were performed in different solvents in order to observe the influence of its polarity in the optical activity of the C_3 compound. For these studies, chloroform, 1,4-dioxane, methylcyclohexane and dodecane have been chosen, were the degree of solvent polarity ranges from the chloroform, as the most polar one, to the dodecane, as the most apolar.[35]

Solutions of C_3-[Zn-(*R,R,R*)-**2**] in each solvent were prepared (at a concentration 5 μM), and CD spectra were recorded in a range of temperatures (different for each solvent) after one heating and cooling cycle to probe the assembly under equilibrium conditions. All of the experiments were performed by performing heating cooling cycles.

3.4.1. Self-assembly studies in chloroform and 1,4-dioxane solutions.

The temperature studies (in the range 263 to 333 K) in CD of the compound C_3-[Zn-(*R,R,R*)-**2**] in a 5 μM solution in $CHCl_3$ showed a non-dependence behavior of the aggregation state (Figure 9).

As shown by the CD spectra, the optical activity of the C_3 compound did not change with temperature, meaning that even though the compound does not present high optical activity, it was stable in front of this external stimulus. The negative Cotton effect with negative maxima at around 430 nm, observed in the CD spectra, suggested an interaction between the porphyrin units as a left-handed aggregate. Moreover, the corresponding absorption spectra did not present significant changes during the temperature studies. Although at 263 K and 333 K the Soret band was observed less intense and shifted to the blue region, the results suggest that this difference in the absorption band could come from an external factor and is not directly related to the kind of supramolecular architecture formed.

(34) Hoeben, J. F. M.; Jonkheijm, P.; Meijer, E. W.; Schenning, A. P. H. J. *Chem. Rev.* **2005**, *105*, 1491-1546.
(35) http://murov.info/orgsolvents.htm

Figure 9. Variable temperature CD spectra and corresponding absorption signals from the CD spectrometer for the compound *C*$_3$-[Zn-(*R,R,R*)-**2**] in $CHCl_3$ (5 μM).

When the CD spectra were registered at temperatures comprised between 283 K to 333 K in a 5 μM solution in 1,4-dioxane, a weak optical activity was observed (Figure 10).

As in the case of chloroform, the self-assembly did not show a clear dependency with the temperature. However, as the temperature rises to 323 K a small decrease in the optical activity for the *C*$_3$ compound was observed. The corresponding absorption spectra showed a maximum absorption at around 427 nm that corresponded to the 0 signal in the CD spectra.

Figure 10. Variable temperature CD spectra and corresponding absorption signals from CD spectrometer for compound C_3-[Zn-(*R,R,R*)-**2**] in 1,4-dioxane (5 μM).

Figure 11shows the comparison of the CD spectrum at room temperature of C_3-[Zn-(*R,R,R*)-**2**] in chloroform and 1,4-dioxane in a 5 μM solution.

It is important to mention, that the self-assembly of compound C_3-[Zn-(*R,R,R*)-**2**], in this two solvents, was not driven by the π-π stacking of the bipyridine moieties because the lack of any CD signal coming from the π-π* transition of these units that should appear from 360 nm to 390 nm.[36] Therefore one could suggested that the optical activity come from porphyrin-porphyrin interactions.

(36) Palmans, A. R. A.; Vekemans, J. A. J. M.; Havinga, E. E.; Meijer, E. W. *Angew. Chem. Int. Ed. Engl.* **1997**, *36*, 2648-2651.

Figure 11. CD spectra from CD spectrometer for compound C_3-[Zn-(*R,R,R*)-**2**] in $CHCl_3$ and 1,4-dioxane (5 μM) at room temperature.

3.4.2. Self-assembly studies in methylcyclohexane and dodecane solutions.

A 5 μM solution of C_3-[Zn-(*R,R,R*)-**2**] in methylcyclohexane was analyzed at different temperatures by CD spectroscopy.

In Figure 12 a strong negative bisignate CD signal was observed with maxima at 437 nm and 430 nm that indicated electronic transitions between the chromophoric rings. The corresponding absorption spectra show a broad Soret band with maximum absorption at 431 nm. The broadening of the Soret band suggested the contribution of two different species, corroborated by the shoulder observed at around 421 nm.

As it was observed for the other two solvents, the aggregation in methylcyclohexane did not present dependence with the temperature either. Nevertheless, the optical activity is much higher when C_3-[Zn-(*R,R,R*)-**2**] was analyzed in the later solvent, indicating that the polarity of the solvent influences the self-assembly of the discotic molecule.

Figure 12. Variable temperature CD spectra and corresponding absorption signals from CD spectrometer for compound C_3-[Zn-(*R,R,R*)-**2**] in methylcyclohexane (5 μM).

The CD spectra and the corresponding absorption spectra at different temperatures of the C_3-[Zn-(*R,R,R*)-**2**] at 5 μM solution in dodecane showed a slight different behavior in its self-assembly compared with the other solvents (Figure 13).

In contrast with the self-assembly observed by CD with the other three solvents, the self-assembly of C_3-[Zn-(*R,R,R*)-**2**] in dodecane showed a temperature dependence, presenting a significant optical activity even at 333 K.

The CD spectra showed a clear negative Cotton effect with maximum CD signal at 437 nm and 432 nm as it was the case of the methylcyclohexane solution. However, at low temperatures a positive band was observed at 426 nm, suggesting that different interactions play a role in the self-assembly process.

Furthermore, if one takes a look to the corresponding absorption spectra, a clear red shift was observed for the Soret band as the temperature decreases.

Figure 13. Variable temperature CD spectra and corresponding absorption signals from the CD spectrometer for the compound C_3-[Zn-(*R,R,R*)-**2**] in dodecane (5 μM).

When the CD spectra at room temperature at 5 μM solution in methylcyclohexane and dodecane were compared, it can be observed that there was no contribution of the π-π stacking of the bipyridine in the self-assembly of the C_3 discotic molecule (Figure 14).

Figure 14. CD spectra from CD spectrometer for compound C_3-[Zn-(*R,R,R*)-**2**] in methylcyclohexane and dodecane (5 μM) at room temperature.

3.4.3. Self-assembly comparison of C_3-[Zn-(*R,R,R*)-2] at room temperature.

As explained before, C_3-[Zn-(*R,R,R*)-**2**] forms an aggregate driven by π-π interactions between the metalloporphyrin ring in all the solvents used, but some difference in the optical activity and band position have been observed (Figure 15).

Chloroform is the most polar solvent where the C_3 compound can be complete soluble. The polar character for this solvent in principle does not favor the self-assembly; even so, the C_3 compound aggregates in a chiral manner as the low optical activity suggests. In the case of dioxane, a solvent that in principle should favor the aggregation, the observed weak optical activity indicates that discreet aggregates were formed.

The optical activity observed in the CD spectra when was recorded from solutions in methylcyclohexane and dodecane was much stronger than for the other two solvents (with higher polarity), meaning that the polarity was an important factor for the self-assembly of this symmetric molecule.

It is important to note that the Cotton effect observed for methylcyclohexane and dodecane were red shifted compared with the solutions of chloroform and 1,4-dioxane. These results suggest that more electronic transitions were involved in the aggregate meaning that a larger architecture was formed.

Figure 15. CD spectra from the CD spectrometer for the compound C_3-[Zn-(*R,R,R*)-**2**] at room temperature.

Commonly, the families of C_3 symmetric molecules based on the benzene-1,3,5-tris(amido-bipy) cores self-assemble through π-π stacking of the bipyridine units rigidified around the central core by intramolecular hydrogen-bondings.[10] However, the C_3 compound synthesized here, with zinc (II) porphyrins in the surroundings of the central core, tend to aggregate through the interaction of the chromophoric rings. This feature could be possibly related to the fact that the porphyrin units, possessing a more extended π system and planar conformations, engage more efficiently in π-π-interactions than the benzene-tris(bipy), thus directing the self-assembly process.

3.5. Study of the hierarchy organization of C_3-[Zn-(*R,R,R*)-2] on surface by AFM.

The discotic molecule C_3-[Zn-(*R,R,R*)-**2**] studied in different solvent solutions (5 μM) were deposited on solid supports by drop casting allowing the solvent to evaporate and finally the material was investigated AFM by using the tapping mode.

A number of parameters play important roles in the process of transferring the self-assemble molecules from solution to a solid support such as molecule-molecule or molecule-surface interactions, as well as the solvent-surface interaction and evaporation rates[37]. The nature of the surface is also an important factor to take into account to successfully adsorb the aggregates in a controlled way.[38]

In this work different surfaces were used to study the hierarchy organization of the C_3 molecules when one drop of solutions of compound C_3-[Zn-(*R,R,R*)-**2**] in the solvents used in previous section: chloroform, dioxane, methylcyclohexane and dodecane.

Highly oriented pyrolitic graphite (HOPG) was chosen for its hydrophobic character, which favors the van der Waals interactions between the surface and the long alkyl chains at the periphery of the porphyrin ring.[39] On the other hand, a hydrophilic surface such as mica that could interact with the core of the C_3 through the amide groups was tested.[40,41]

3.5.1. Study of the hierarchy organization from chloroform solution.

One drop of C_3-[Zn-(*R,R,R*)-**2**] in chloroform (5 μM solution) was drop-casted onto highly oriented pyrolitic graphite (HOPG) at room temperature and different areas of the surface were scanned (Figure 16). The AFM images of the resulting material showed that the entire surface was covered uniformly by globular objects of different sizes. Moreover, the close-up images (b, c and d) showed that sheet like structures were adsorbed over the surface. The different sizes of the globular objects might be related to the presence of non-aggregated molecules in solutions, as well as different sizes of the aggregates. Furthermore, the planar objects observed on the surface might be due to the different interactions molecule-molecule and molecule- surface because of the affinity of the alkyl chains with the graphite surface.

(37) Su, Y.; Gao, X.; Liu, J.; Xing, R.; Han, Y. *Phys. Chem. Chem. Phys.* **2013**, *15*, 14396-14404.
(38) Jonkheijm, P.; Hoeben, F. J. M.; Kleppinger, R.; Van Herrikhuyzen, J.; Schenning, A. P. H. J.; Meijer, E. W. *J. Am. Chem. Soc.* **2003**, *125*, 15941-15949.
(39) De Feyter, S.; De Schryver, F. C. *Chem. Soc. Rev.* **2003**, *32*, 139-150.
(40) Nakagawa, T.; Ogawa, K. Langmuir **1994**, *10*, 525-529.
(41) Tiberg, F.; Brinck, J.; Grant, L. *Curr. Opin. Colloid Interface Sci.* **2000**, *4*, 411-419.

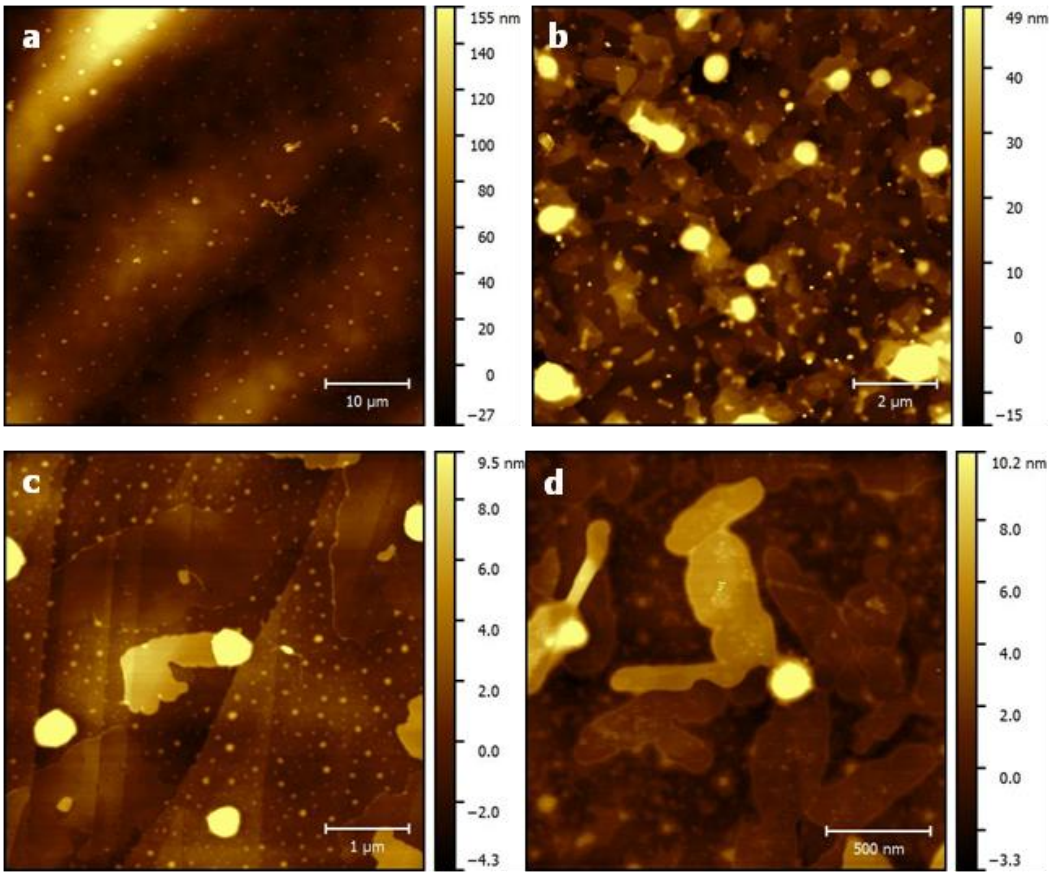

Figure 16. Tapping mode AFM images of one drop of C_3-[Zn-(*R,R,R*)-**2**] (5 µM) on freshly cleaved HOPG.

As Figure 17 shows, the big globular objects corresponding to the self-assemble C_3-[Zn-(*R,R,R*)-**2**] molecules present a height around 30 nm as indicated by the profile. As mentioned before, small spherical objects were also present on the surface, presenting heights of around 4 nm as showed by profile 2. These results suggest that the small particles could correspond to the effective packing of few molecules of C_3-[Zn-(*R,R,R*)-**2**], that might come directly from the solution or these small aggregates, were part of a bigger architecture that has been partially destroyed by the molecule-surface interaction. Moreover, the nanosheets with irregular forms presents heights from 2 nm to 4 nm, that could be formed during the evaporation process of the solvent, where other non-covalent interactions could be involved in the packing of the planar structure.[42]

(42) Hou, X.; Schober, M.; Chu, Q. *Cryst. Growth. Des.* **2012**, *12*, 5159-5163.

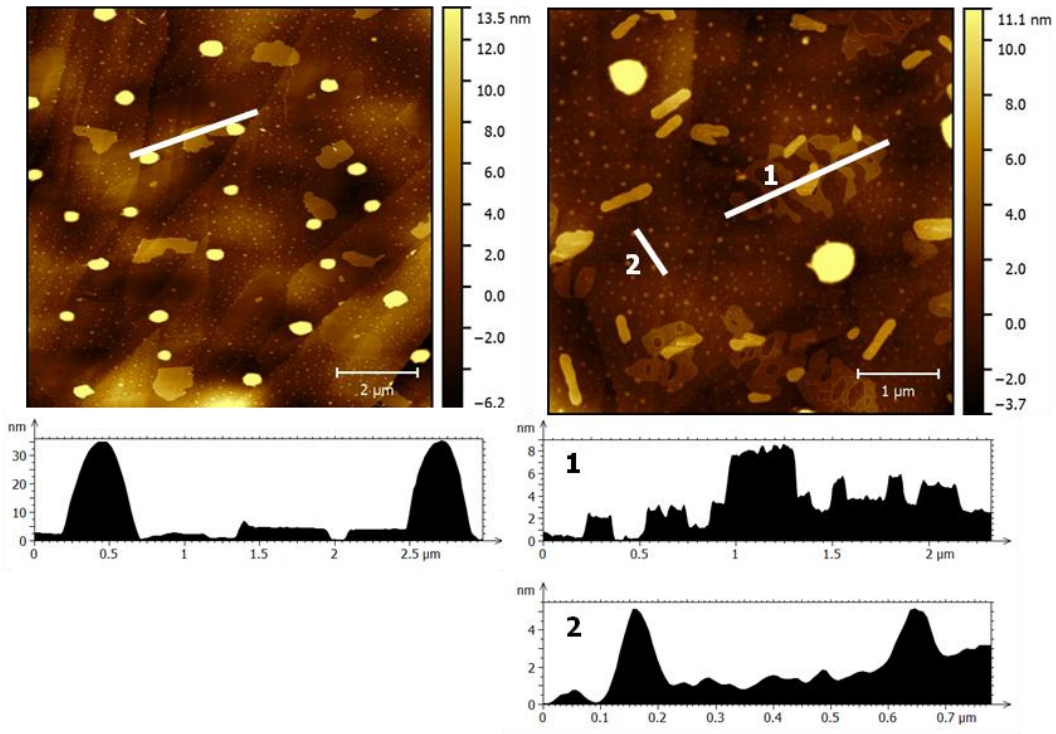

Figure 17. Tapping mode AFM images of one drop of C_3-[Zn-(*R,R,R*)-**2**] (5 µM) on freshly cleaved HOPG.

When the same chloroform solution was deposited onto mica surface, similar objects were observed in the AFM topographic images. Images (a) and (b) of Figure 18 show larger scan areas where two sizes of round objects were observed. In image (a) a kind of alignment can be observed for the globular objects, even though, the close-up image of this scans area shows a non-perfect order for the structures (Figure 18c).

If one takes a look to the profiles of both regions, clearly the heights of the globular objects differ considerably between them. The profile extracted in image (c) indicates objects of around 80 nm heights whereas the globular objects in image (d) were much higher, showing height close to 200 nm. Is quite surprising the huge difference in height and even in size of the aggregates depending of the area study. These results can be explained by the different concentration gradient during the evaporation process as the relative concentration increases the vertical columnar structure growth.

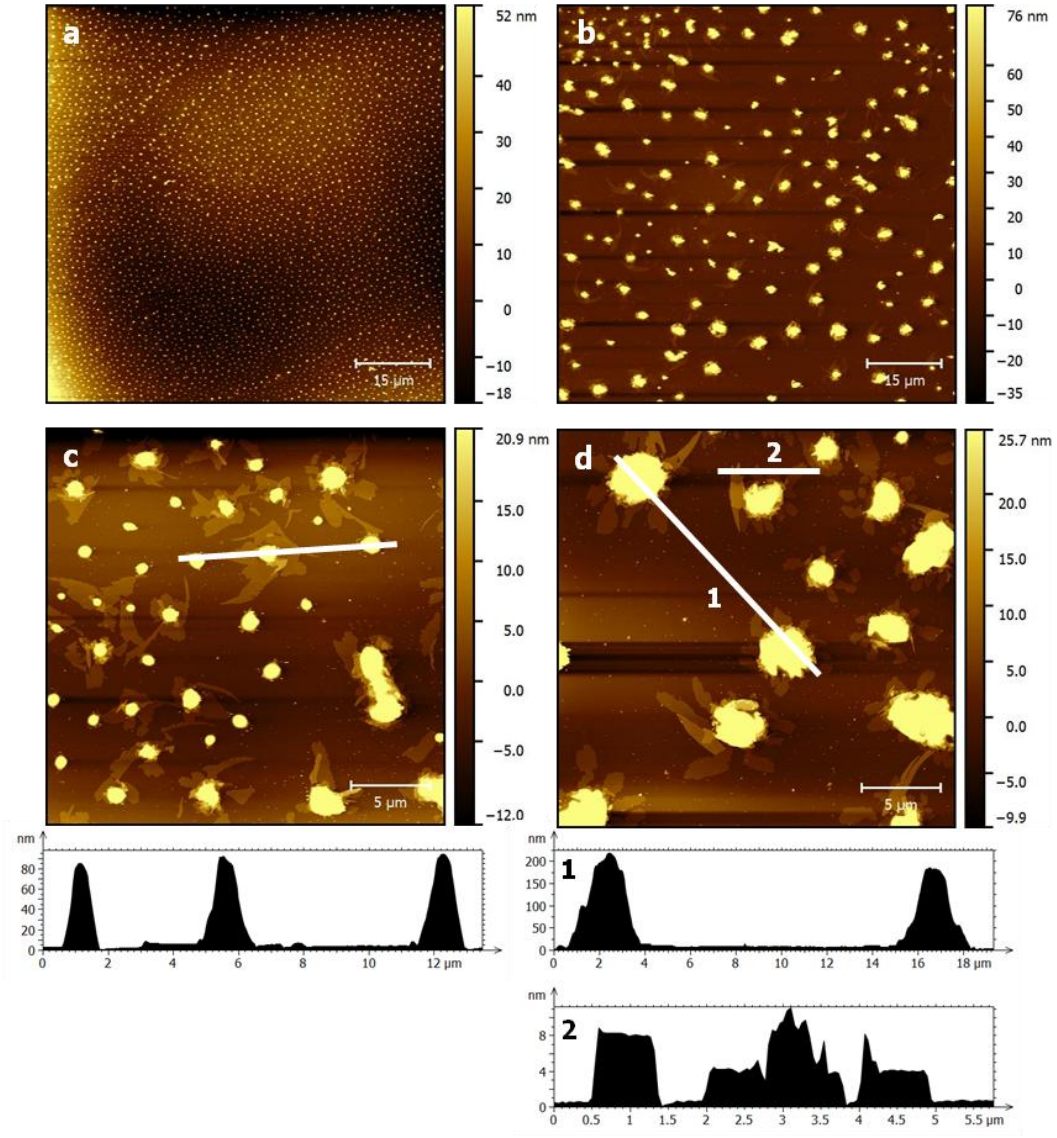

Figure 18. Tapping mode AFM images of one drop of C_3-[Zn-(*R,R,R*)-**2**] (5 µM) on freshly cleaved mica.

Is important to remark that nanosheets were also observed underneath of the globular structures with heights of around 4 nm. This observation suggests that the planar objects can be formed in the evaporation process instead of being transferred from the solution.

It is necessary to emphasize the huge difference in heights of the columnar aggregates when they are adsorbing to the graphite surface or on the hydrophilic surface. A plausible explanation for the big aggregates observed on mica relies in the poor affinity between the C_3 and the surface, where the molecules tend to growth perpendicular to the hydrophilic surface.

3.5.2. Study of the hierarchy organization from 1,4-dioxane solution.

A 5 μM solution of C_3-[Zn-(*R,R,R*)-**2**] in 1,4-dioxane was drop casted onto HOPG and the solvent was evaporated under ambient conditions. Immediately after, different areas of the graphite surface were analyzed in tapping mode offering images as the ones observed in Figure 19.

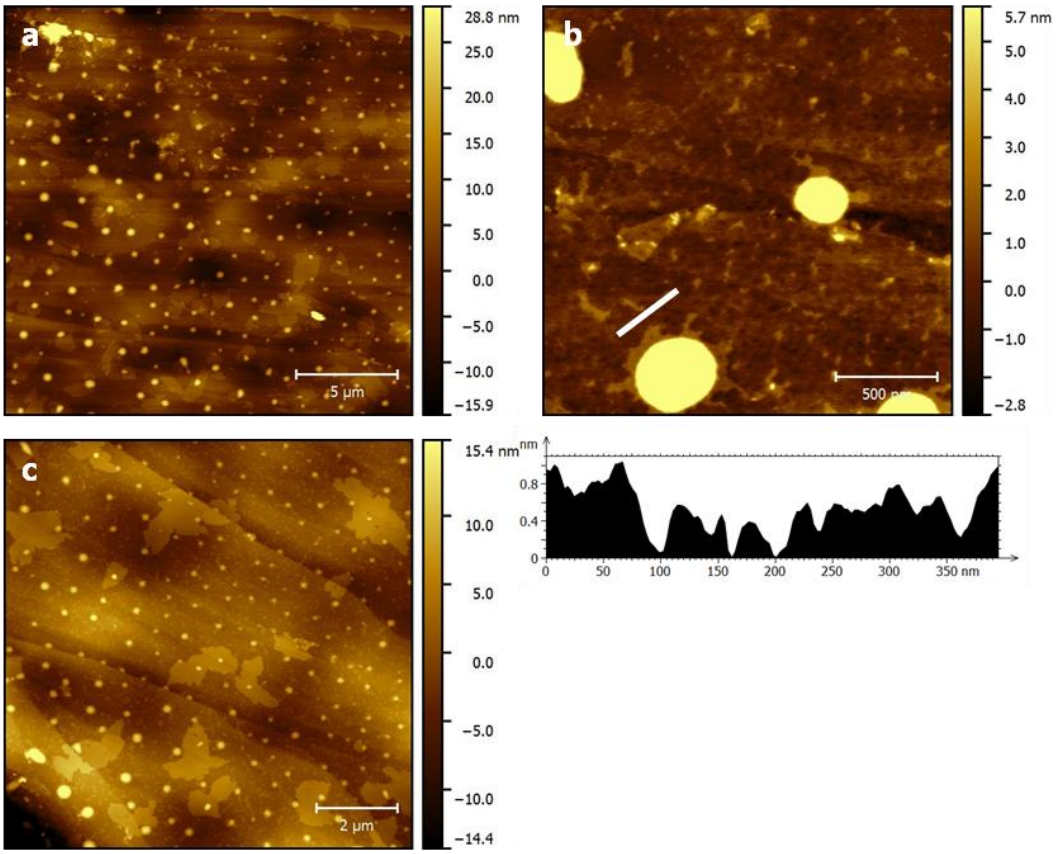

Figure 19. Tapping mode AFM images of one drop of C_3-[Zn-(*R,R,R*)-**2**] (5 μM) on freshly cleaved HOPG.

The pictures show globular objects corresponding to the C_3-[Zn-(*R,R,R*)-**2**] aggregates all over the surface. Moreover, as it can observe in the image (19b), a non-ordered layer seemed to cover the entire surface with heights in the range of 0.4 nm to 1 nm, that may correspond to isolated molecules.

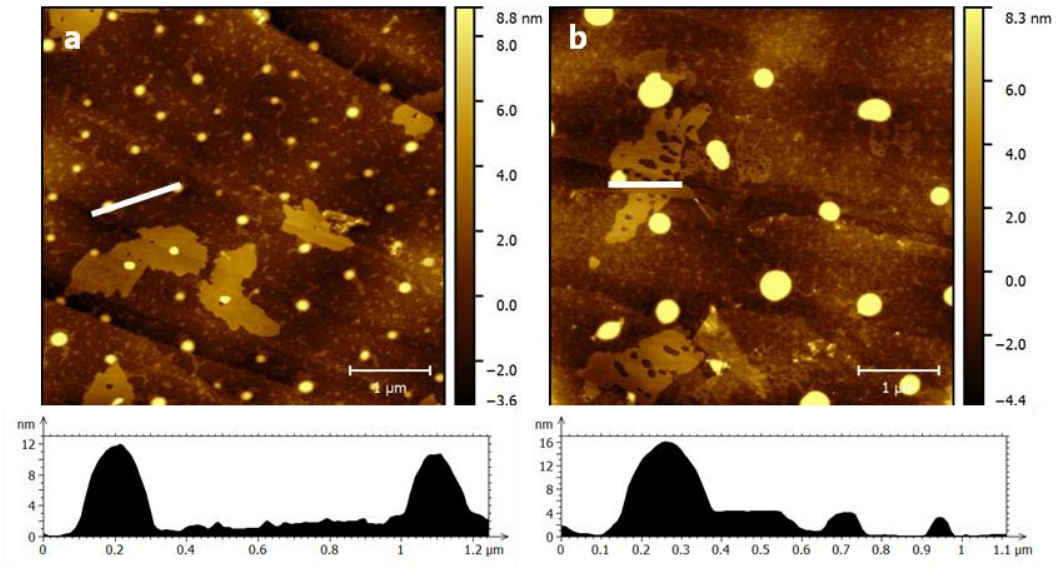

Figure 20. Tapping mode AFM images of one drop of C_3-[Zn-(*R,R,R*)-**2**] (5 µM) on freshly cleaved HOPG.

It should be noticed that the globular objects observed in Figure 20 present heights of 12-16 nm as the profile indicated, that were a slightly smaller than those observed for the structures in $CHCl_3$ on the same surface. These results suggest that the evaporation rate influences the size of the hierarchical architecture, being slower for the dioxane solution. Furthermore, as observed previously, nanosheets of 4 nm height were present on the HOPG surface, corroborating that these structures were formed independently of the solvent and the surface.

Finally, one drop of the 1,4-dioxane solution of the C_3-[Zn-(*R,R,R*)-**2**] compound was deposited onto a mica surface (Figure 21). Images (a) and (b) show 80x80 µm area scan with different sizes of the globular stacks. The profile in image (a), shows objects of around 200 nm height while image (c) indicates that heights are approximately 80 nm heights for all the objects. Such heights are in concordance with the ones observed in chloroform, therefore, it seems that the nature of the solvent does not affect in the hierarchy organization of the C_3-[Zn-(*R,R,R*)-**2**] on the hydrophilic surface.

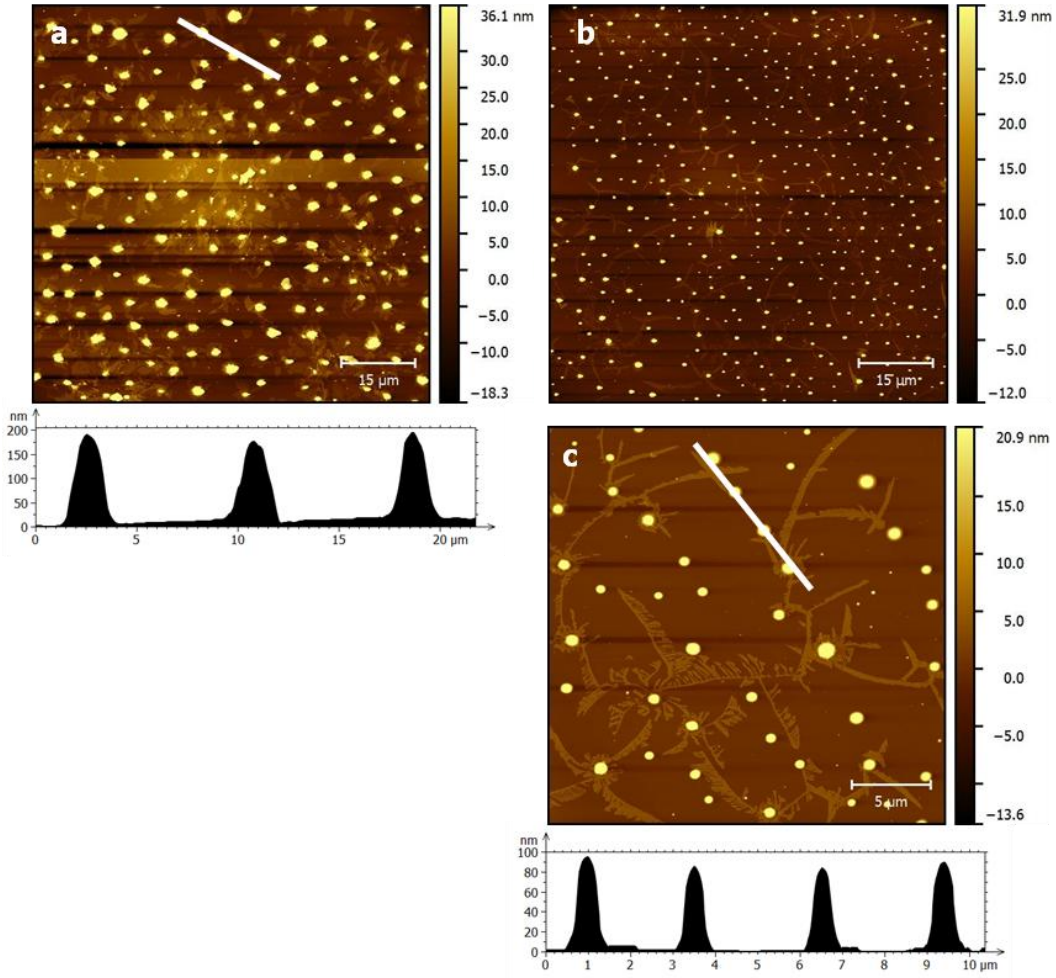

Figure 21. Tapping mode AFM images of one drop of C_3-[Zn-(*R,R,R*)-**2**] (5 µM) on freshly cleaved mica.

It should to be taken into consideration, that no layer of isolated C_3-[Zn-(*R,R,R*)-**2**] symmetric molecules was clearly observed in the topographic images, which is consistent with the nature of the surface. Therefore, it confirms that molecule-molecule interactions are stronger than molecule-surface.

It is worthy to mention that a planar structure was also formed under these conditions, even though they as appear as branches instead of more rectangular sheets. In spite, their heights of 4 nm were in agreement with the ones observed before (Figure 22).

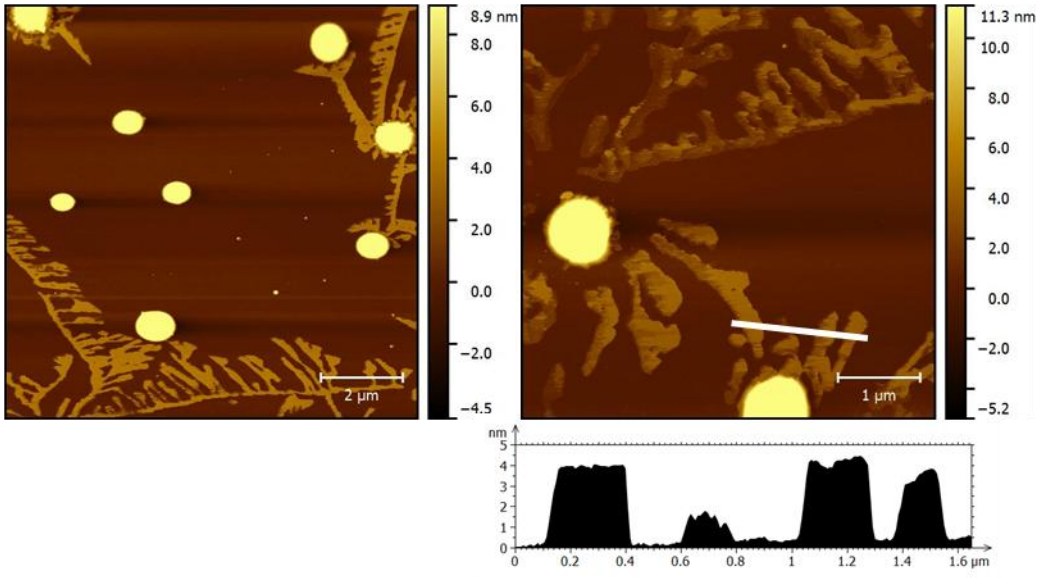

Figure 22. Tapping mode AFM images of one drop of C_3-[Zn-(*R,R,R*)-**2**] (5 µM) on freshly cleaved mica.

3.5.3. Study of the hierarchy organization from methylcylcohexane solution.

When one drop of C_3-[Zn-(*R,R,R*)-**2**] in methylcyclohexane solution was deposited onto the HOPG surface globular objects were observed with heights around 10 nm as it can be observed in the profile in Figure 23b. Furthermore image (b) also shows a regular layer that covered the entire surface with a height of approximately 0.8 nm.

If one takes a careful look to the underneath layer, objects with a shape of needles seemed to cover the graphite surface, contrary to the dioxane solution, where the layer observed displayed non-organized structures.

Not surprisingly, sheet like objects were present on the surface, as observed for the images studied before, indicating once more that the observation of the planar structure was independent of solvent and surface.

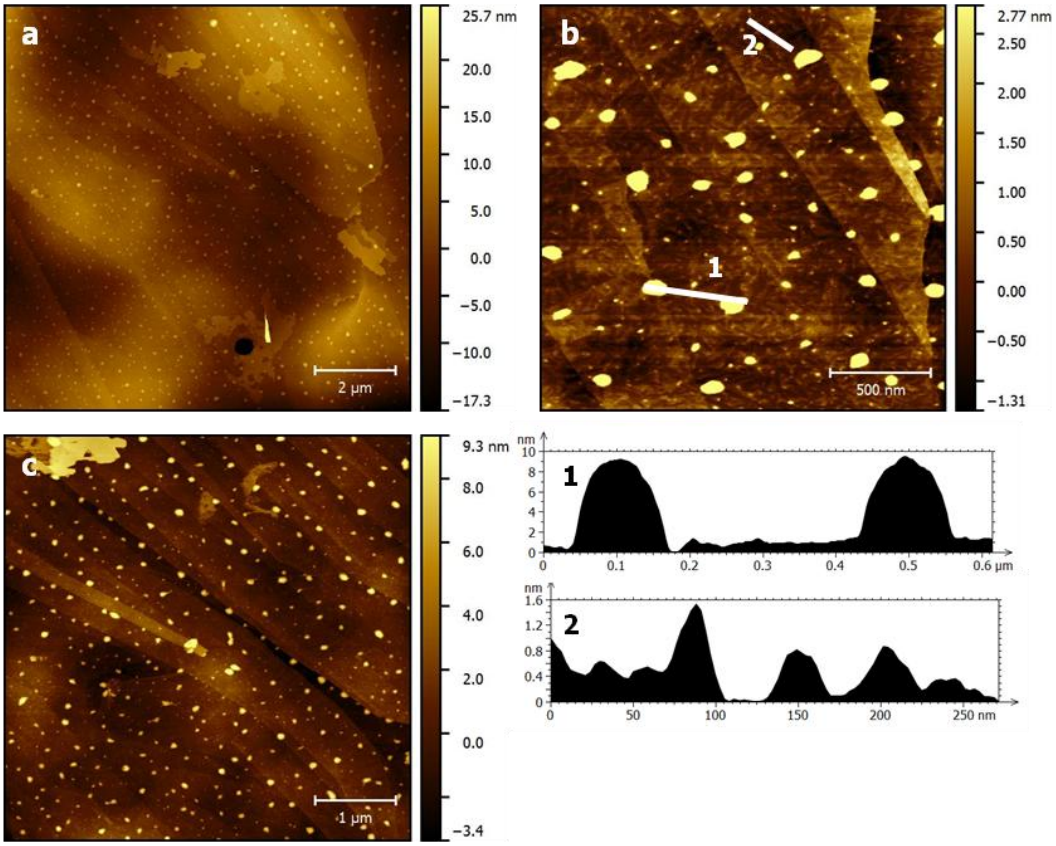

Figure 23. Tapping mode AFM images of one drop of C_3-[Zn-(*R,R,R*)-**2**] (5 µM) on freshly cleaved HOPG.

Figure 24 shows the hierarchy organization of C_3-[Zn-(*R,R,R*)-**2**] when one drop of the methylcyclohexane solution was drop casted onto mica. As observed for the other solvents, when the aggregates were studied on mica surface, these were present as bigger objects compared with the ones observed on the hydrophobic surface.

As the profiles of images (b) and (c) show, the structures present heights of around 100 nm, that were in concordance with the heights observed previously for chloroform and 1,4-dioxane solutions. However, it indicates that the slower evaporation rate for methylcylohexane compared with the other two solvents, might give place to the observation of a more uniform height for the globular objects.

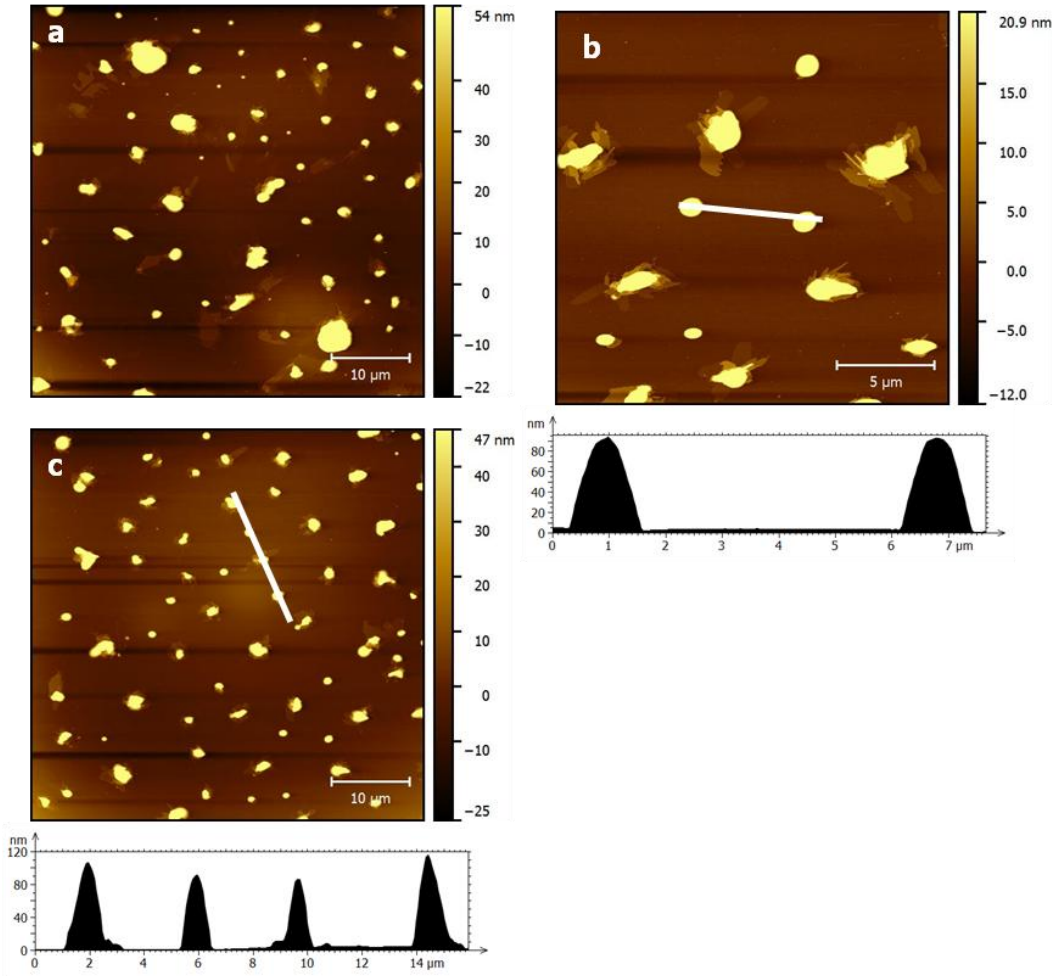

Figure 24. Tapping mode AFM images of one drop of C_3-[Zn-(*R,R,R*)-**2**] (5 µM) on freshly cleaved mica.

3.5.4. Study of the hierarchy organization from dodecane solution.

When one drop of dodecane solution was deposited on graphite surface, only a layer of small particles were observed and some isolated bigger object was present on the entire surface as shown in Figure 25.

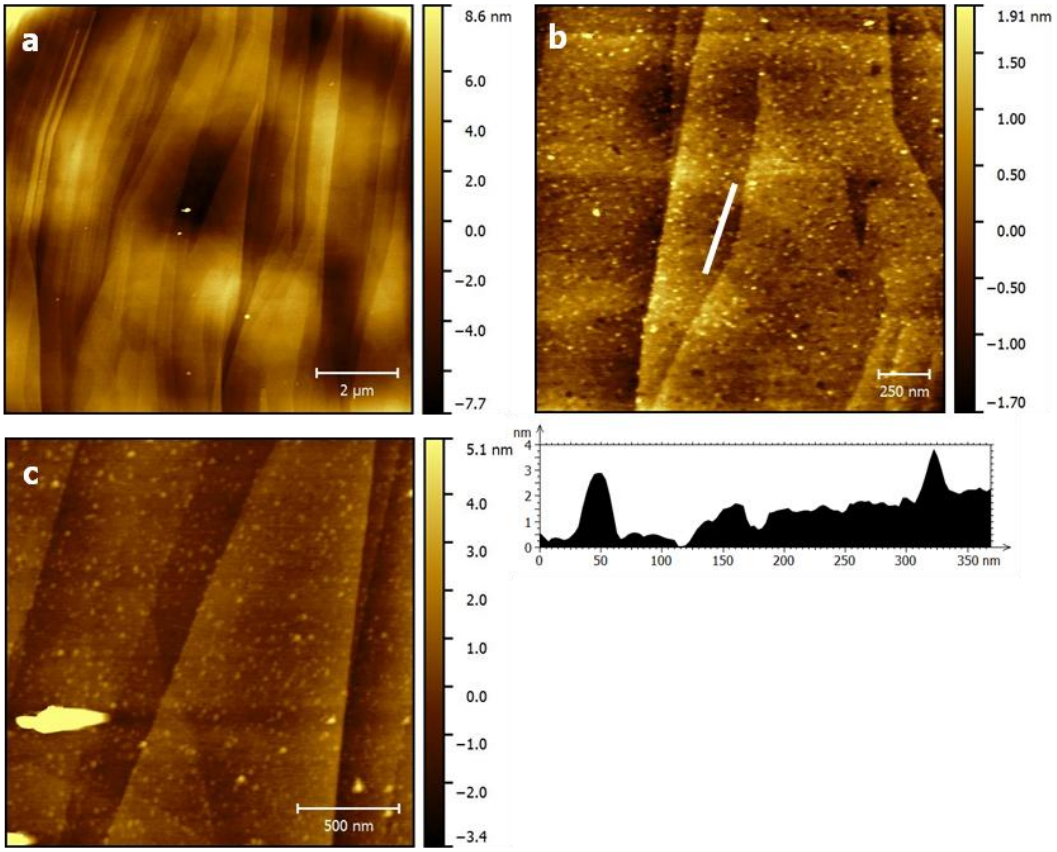

Figure 25. Tapping mode AFM images of one drop of C_3-[Zn-(*R,R,R*)-**2**] (5 µM) on freshly cleaved HOPG.

The profile shown in image (b) clearly depicts that the surface was covered by a layer and small objects that have heights of approximately 3 nm, much smaller than the ones observed before.

As pointed out previously, these results suggest that, the evaporation rate is an important factor to take into account for the hierarchy organization of the columnar stacks.

It is necessary to emphasize that the solvent dodecane presents a high viscosity value, making difficult to scan properly the sample, even working the tapping mode, the tip was sticking to the surface.

When the dodecane solution was adsorbed to the mica surface, the measurements of the hierarchy organization for the objects became harder than the other solvents, due to the surface-solvent interaction. The low affinity of the dodecane with the hydrophilic surface did not allow the spread of the solvent over the mica surface (Figure 26).

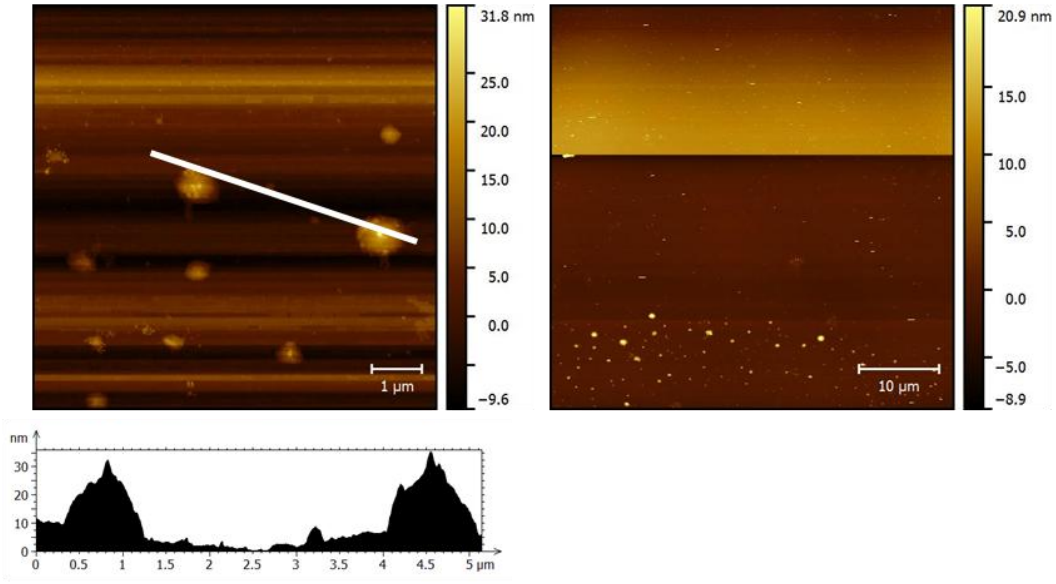

Figure 26. Tapping mode AFM images of one drop of C_3-[Zn-(*R,R,R*)-**2**] (5 µM) on freshly cleaved mica.

The profile in Figure 26 shows a height of around 30 nm for the globular objects observed, confirming that the slow evaporation for this solvent influences dramatically the growth of the columnar stacks.

3.6. Conclusions.

It has been shown that a chiral C_3-[Zn-(*R,R,R*)-**2**] discotic molecule self-assemblies in different solvents through π-π interactions between the porphyrin rings instead of the π-π interactions between the central core of the C_3 molecules. Moreover, the influence of the polarity of the solvents on the optical activity of the columnar stacks has been demonstrated by CD.

It is necessary to note, that the hierarchy organization of the C_3-[Zn-(*R,R,R*)-**2**] aggregates observed by AFM when they were transferred from solution to a solid support was dependent of the nature of the surface and the boiling point of the solvent. Therefore, the vertical size of the supramolecular architecture was smaller when the solutions were deposited onto HOPG due to the van der Waals interactions among molecule-surface, whereas the hydrophilicity of the mica surface favors the perpendicular growth of the aggregate because molecule-molecule interactions are stronger than molecule-surface interactions.

3.7. Experimental section.

NMR spectra : The nuclear magnetic resonance spectra were recorded in a Bruker AVANCE^{II} 300 and Bruker Avance DRX 300.

LDI-TOF : Mass spectroscopy performed with an Ultraflex (TOF/TOF) spectrometer.

MALDI-TOF MS: Spectra were recorded on Bruker Biflex-IIITM apparatus, equipped with a 337 nm N_2 laser.

FT-IR measurements : All FTIR measurements were recorded in Perkin Elmer (Spectrum one). The samples were of solid compounds (recovered after evaporation of solvent in a non-controlled precipitated way) and were performed in attenuated total reflection (ATR) mode. The samples were measured on the plate of universal ATR (UATR).

Atomic Force Microscopy (AFM) : Topographic AFM images were acquired in the dynamic tapping mode using a FORT Si tip in the *Servei de AFM of the ICMAB* in a Agilent 5100 microscope. Solutions of C_3-[Zn-(*R,R,R*)-**2**] were drop-casted onto HOPG surface or mica surface and measurements were performed at ambient conditions. The color code in all the images shown is such that dark are lower and bright are higher values of the height.

CD measurements : A Jasco J-275 spectropolarimeter was used for CD spectra measurements. A Peltier-temperature programmer for thermosettting the samples was used to cool the solutions. The solutions were prepared by diluting a solid sample of the C_3-[Zn-(*R,R,R*)-**2**] in the corresponding amount of the solvent and the solution was heated until all the compound had dissolved to obtain a 5 μM as final concentration. The sample was transferred to a quartz cuvette of 1 cm length to be analyzed. When the measure temperature was reached and stabilized, spectra were recorded.

UV-Visible absorption measurements : UV-Visible absorption measurements were performed using a UV-Vis-NIR Varian, model Cary 5 instrument using a 1 cm length quartz cells. All the samples were prepared, diluting a solid sample of the C_3-[Zn-(*R,R,R*)-**2**] in the corresponding amount of the solvent. The solution was heated until all the compound had dissolved to obtain a 5 μM as final concentration.

Materials : Compound (*R*)-**3** was prepared as described previously.

3.7.1. Synthesis of (*R*)-Methyl 2-(4-formylphenoxy)propanoate (*R*)-3

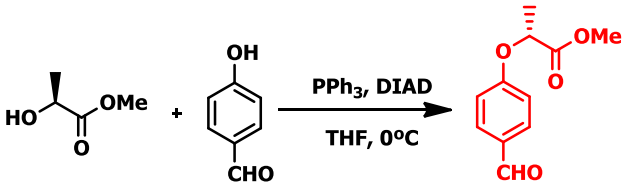

(*R*)-3

4-hydroxy-benzaldehyde (4.00 g, 32.75 mmol), *S*-(-)-methyl lactate (3.75 ml, 39.31 mmol) and triphenylphosphine (10.30 g, 39.31 mmol) were dissolved in anhydrous THF (140 ml). The mixture was stirred vigorously at 0ºC and under Ar atmosphere for 10 minutes. A second solution of diisopropylazodicarboxylate (7.70 ml, 39.31 mmol) in anhydrous THF (25 ml) was added dropwise over 30 minutes. The resulting solution was stirred overnight at room temperature. H_2O was added in order to quench the reaction and then the solvent was removed under pressure. The aqueous solution was extracted with CH_2Cl_2 (3x25 ml) and the organic phase was dried over $MgSO_4$ anhydrous. Finally, the organic solvent was filtered through cotton wool and evaporated to give yellow oil. The crude compound was purified by silica gel column chromatography (hexane/EtOAc, 8:2) to obtain 5.38 g (79 %) of the desired compound (*R*)-**3**. **M.F. :** $C_{11}H_{12}O_4$; **M.W. :** 208.22 g/mol ; **^{1}H-NMR** (250 MHz, *d*-Chloroform) δ 9.80 (s, 1H; CHO), 7.74 (d, J = 8.6 Hz, 2H; ArH), 6.90 (d, J = 8.8 Hz, 2H; ArH), 4.82 (q, J = 6.8 Hz, 1H; O<u>CH</u>(CH_3)), 3.69 (s, 3H; $COOCH_3$), 1.59 (d, J = 6.8 Hz, 3H; OCH(<u>CH_3</u>)) : **$[\alpha]_{546literature}$ =** +46 deg·cm^2/mg, **$[\alpha]_{546observed}$ =** +43 deg·cm^2/mg (c=0.19 M; CH_2Cl_2).

3.7.2. Synthesis of 4-etoxy-benzaldehyde 4 and 4-octadecaneoxy-benzaldehyde 5

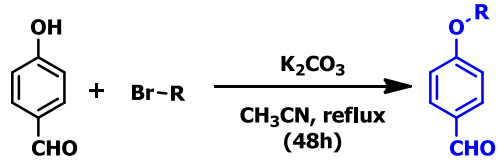

4 ; R=C_2H_5
5 ; R=$C_{18}H_{37}$

4-hydroxy-benzaldehyde (4.00 g, 32.75 mmol) and K_2CO_3 (13.60 g, 98.25 mmol) were dissolved in acetonitrile (82 ml) and the solutions was stirred at room temperature further 1 hour. The corresponding 1-bromo alkyl (32.75 mmol) was added to the aldehyde solution and the mixture was stirred at reflux further 48 hours. For compound **4**, the crude solution was filtrate and evaporated under pressure to obtain 4.4 g of a yellow-brownish oil (90.4 %). For compound **5** the

solution was filtrate in warm conditions, and the resulting solution was cooled down at room temperature since a precipitate was appeared. The desired white solid was filtrated in a porcelain filter funnel and dried to obtain 4.48 g (83.3 %).

4-etoxy-benzaldehyde 4 : M.F. : $C_9H_{10}O_2$; **M.W. :** 164.20 g/mol ; **^{1}H NMR** (250 MHz, *d*-Chloroform) δ 9.77 (s, 1H; CHO), 7.72 (d, *J* = 8.9 Hz, 2H; ArH), 6.88 (d, *J* = 8.8 Hz, 2H; ArH), 4.00 (q, *J* = 7.0 Hz, 2H; $O\underline{CH_2}CH_3$), 1.35 (t, *J* = 7.0 Hz, 3H; $OCH_2\underline{CH_3}$).

4-octadecaneoxy-benzaldehyde 5 : M.F. : $C_{25}H_{42}O_2$; **M.W. :** 374.62 g/mol ; **^{1}H NMR** (250 MHz, *d*-Chloroform) δ 9.88 (s, 1H; CHO), 7.83 (d, *J* = 8.8 Hz, 2H; ArH), 6.99 (d, *J* = 8.7 Hz, 2H; ArH), 4.04 (t, *J* = 6.5 Hz, 2H; $O\underline{CH_2}CH_2(CH_2)_{15}CH_3$), 1.81 (dt, *J* = 14.5, 6.6 Hz, 2H; $OCH_2\underline{CH_2}(CH_2)_{15}CH_3$), 1.25 (m, 30H; $OCH_2CH_2(\underline{CH_2})_{15}CH_3$), 0.96-0.83 (m, 3H; $OCH_2CH_2(CH_2)_{15}\underline{CH_3}$).

3.7.3. Synthesis of the chiral free-base porphyrins (*R*)-6 and (*R*)-7.

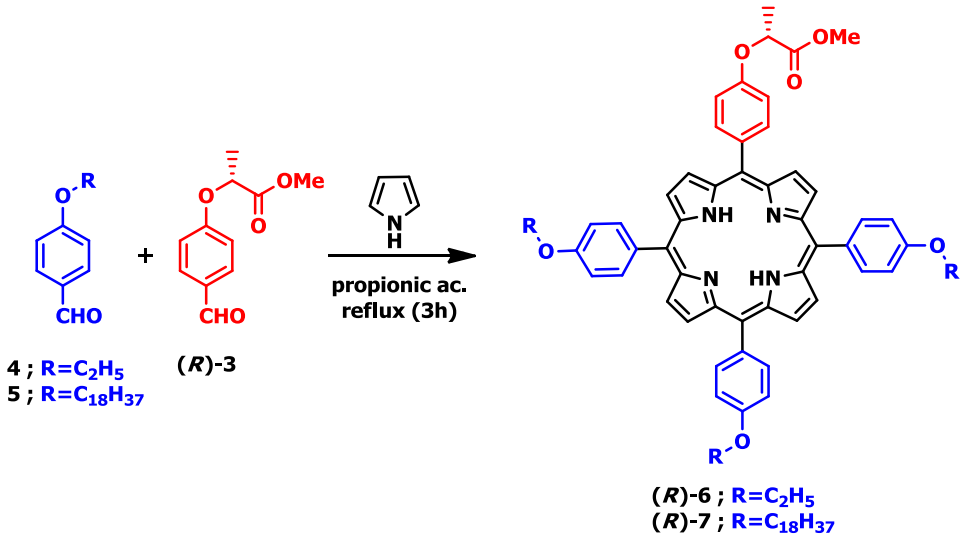

In separate reactions, **(*R*)-3** (300.0 mg, 1.44 mmol) and **4** (0.65 g, 4.32 mmol) or **5** (1.60 g, 4.32 mmol) were dissolved in propionic acid (15 ml) and stirred under reflux for about 30 minutes. A freshly pyrrole (0.40 ml, 5.76 mmol) was added dropwise and the mixture was stirred for 3 hours using reflux in ambient conditions. The solution was cooled down at room temperature and then was extracted with a saturate sodium bicarbonate solution and dried over Na_2SO_4 anhydrous. The solvent was removed under pressure. The crude compound **(*R*)-6** was subjected in a silica gel column chromatography (100% CH_2Cl_2) to obtain 257.5 mg (21.1 %) of the desired porphyrin as a purple solid. On the other hand, the crude compound **(*R*)-7** was subjected in a silica gel chromatography column (7:3 hexane/ CH_2Cl_2) to obtain 347.5 mg (15.3 %) of the desired porphyrin.

5-[4-(*R*)-Methyl-2-phenoxypropionate]-10,15,20-[4-ethoxybenzene] porphyrin (*R*)-6 : M.F. : $C_{54}H_{48}N_4O_6$; **M.W. :** 848.98 g/mol ; **Found LDI-Tof [M^+] :** 849.3 ; **^{1}H NMR** (300 MHz, *d*-Chloroform) δ 8.87 (m, 8H; pyrrole), 8.12 (dd, *J* = 8.5, 4.0 Hz, 6H; PhOCH$_2$CH$_3$; 2H; PhOCH(CH$_3$)CO$_2$CH$_3$), 7.41 – 7.10 (m, 8H; PhOCH$_2$CH$_3$; PhOCH(CH$_3$)CO$_2$CH$_3$), 5.15 – 5.02 (m, 1H; OCH(CH$_3$)), 4.31 (q, *J* = 6.9 Hz, 6H; OCH$_2$CH$_3$), 3.93 (s, 3H; CO$_2$CH$_3$), 1.84 (d, *J* = 6.7 Hz, 3H; OCH(CH$_3$)), 1.62 (t, *J* = 7.0 Hz, 9H; OCH$_2$CH$_3$), -2.73 (s, 2H; NH) ; **UV-Vis** ($CHCl_3$) λ_{max}/nm (ε M^{-1} cm^{-1}) : 422 (480240), 519 (17120), 556 (12072), 595 (5726), 651 (7776).

5-[4-(*R*)-Methyl-2-phenoxypropionate]-10,15,20-[4-octadecaneoxybenzene] porphyrin (*R*)-7 : M.F. : $C_{102}H_{144}N_4O_6$; **M.W. :** 1522.6 g/mol ; **Found LDI-Tof [M^+] :** 1523.3 ; **^{1}H NMR** (300 MHz, *d*-Chloroform) δ 8.86 (m, 8H; pyrrole), 8.11 (d, *J* = 8.5 Hz, 6H; PhOC$_{18}$H$_{37}$), 7.29 (d, *J* = 8.5 Hz, 6H; PhOC$_{18}$H$_{37}$), 7.24 (m, 2H; PhOCH(CH$_3$)CO$_2$CH$_3$), 5.09 (m, 1H; OCH(CH$_3$)), 4.25 (t, *J* = 6.6 Hz, 6H; OCH$_2$CH$_2$(CH$_2$)$_{15}$CH$_3$), 3.92 (s, 3H; CO$_2$CH$_3$), 2.08-1.92 (m, 6H; OCH$_2$CH$_2$(CH$_2$)$_{15}$CH$_3$), 1.83 (d, *J* = 6.7 Hz, 3H; OCH(CH$_3$)), 1.27 (m, 90H; OCH$_2$CH$_2$(CH$_2$)$_{15}$CH$_3$), 0.88 (t, *J* = 6.6 Hz, 9H; OCH$_2$CH$_2$(CH$_2$)$_{15}$CH$_3$), -2.76 (s, 2H; NH) ; **IR-ATR** (cm^{-1}) : 3319 (w, NH), 2922 (s, CH_2), 2848 (s, CH_2), 1766 (m, COOMe), 1746 (m, COOMe), 1606 (m, phenyl), 1506 (m, phenyl), 1238 (s), 963 (s), 799 (s) ; **UV-Vis** (MCH) λ_{max}/nm (ε M^{-1} cm^{-1}) : 420 (353154), 517 (13410), 553 (9478), 594 (4236), 652 (4936).

3.7.4. Synthesis of the chiral metalloporphyrins Zn-(*R*)-6 and Zn-(*R*)-7.

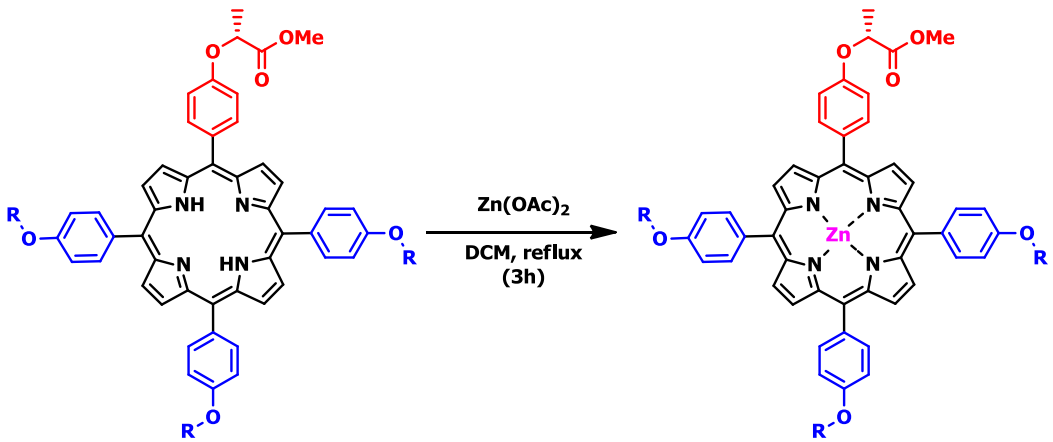

The free-base porphyrin **(*R*)-6** (158.0 mg, 0.19 mmol) and **(*R*)-7** (70.5 mg, 0.046 mmol) in a separate reactions was dissolve in dichloromethane ($7.5 \cdot 10^{-3}$ M) and was stirred at reflux under inert atmosphere. Zn(OAc)$_2$ (3.5 eq) was dissolved in 1:1 mixture of CH_2Cl_2/MeOH (0.052 M) and was added drop wise with syringe over 5 minutes. The reaction mixture was refluxed further three

hours. Dichloromethane was added and the organic layer was washed with a saturated aqueous solution of $NaHCO_3$, brine and was dried over anhydrous Na_2SO_4 and concentrated *in vacuum*. The inpure **Zn-(*R*)-6** was purified by silica gel chromatography (100% CH_2Cl_2) giving 125.2 mg (73.7 %) of the desired metalloporphyrin as a purple metallic powder. For metalloporphyrin **Zn-(*R*)-7** a silica gel chromatography (15:85 ; hexane/$CHCl_3$) was used to purified the compound giving 54.5 mg (74.2%) as a purple metallic powder.

5-[4-(*R*)-Methyl-2-phenoxypropionate]-10,15,20-[4-ethoxybenzene] porphyrin zinc (II) Zn-(*R*)-6 : M.F. : $C_{54}H_{46}N_4O_6Zn$; **M.W. :** 912.35 g/mol ; **^{1}H NMR** (300 MHz, *d*-Chloroform) δ 8.97 (q, *J* = 4.7, 4.0 Hz, 8H; pyrrole), 8.11 (m, 8H; PhOCH_2CH_3; Ph$OCH(CH_3)CO_2CH_3$), 7.26 (m, 8H; PhOCH_2CH_3; Ph$OCH(CH_3)CO_2CH_3$), 5.06 (q, *J* = 6.7 Hz, 1H; O$CH(CH_3)$), 4.33 (q, *J* = 6.8 Hz, 6H; OCH_2CH_3), 3.91 (s, 3H; CO_2CH_3), 1.82 (d, *J* = 6.8 Hz, 3H;

5-[4-(*R*)-Methyl-2-phenoxypropionate]-10,15,20-[4-octadecaneoxybenzene] porphyrin zinc (II) Zn-(*R*)-7 : M.F. : $C_{102}H_{142}N_4O_6Zn$; **M.W. :** 1585.6 g/mol ; **Found LDI-Tof [M^+] :** 1586.2 ; **^{1}H NMR** (300 MHz, *d*-Chloroform) δ 9.05-8.94 (m, 8H; pyrrole), 8.19-8.06 (m, 8H; ArH), 7.31-7.27 (m, 8H; ArH), 5.06 (q, *J* = 6.8 Hz, 1H; O$CH(CH_3)$), 4.26 (t, *J* = 6.5 Hz, 6H; O$CH_2CH_2(CH_2)_{15}CH_3$), 3.92 (s, 3H; CO_2CH_3), 2.07-1.93 (m, 6H; $OCH_2CH_2(CH_2)_{15}CH_3$), 1.83 (d, *J* = 6.8 Hz, 3H; $OCH(CH_3)$), 1.71-1.55 (m, 6H; $OCH_2CH_2CH_2(CH_2)_{14}CH_3$), 1.31 (s, 84H; $OCH_2CH_2(CH_2)_{15}CH_3$), 0.97-0.77 (m, 9H; $OCH_2CH_2(CH_2)_{15}CH_3$) ; **UV-Vis** ($CHCl_3$) λ_{max}/nm (ε M^{-1} cm^{-1}) : 420 (360782), 554 (14284), 596 (3470).

3.7.5. Synthesis of the chiral acid metalloporphyrin Zn-(*R*)-8 and Zn-(*R*)-9.

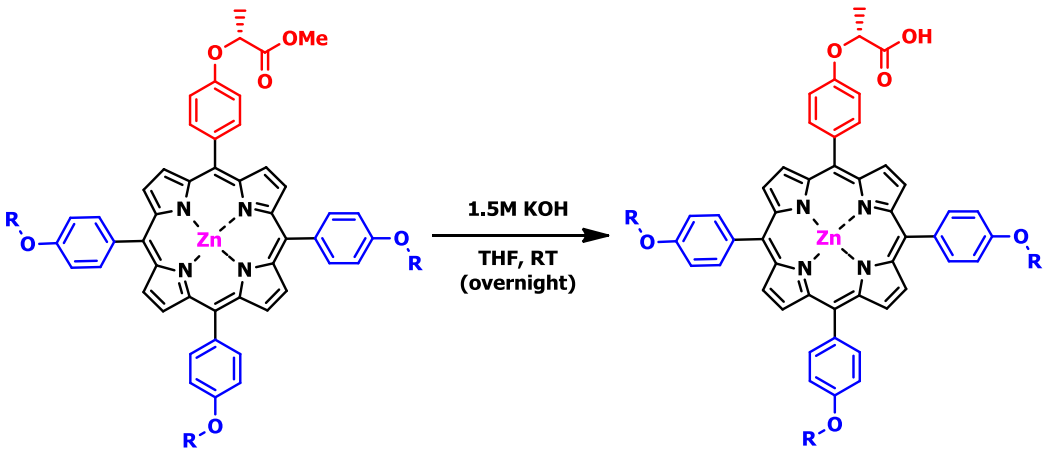

Zn-(*R*)-6 ; R=C_2H_5
Zn-(*R*)-7 ; R=$C_{18}H_{37}$

Zn-(*R*)-12 ; R=C_2H_5
Zn-(*R*)-13 ; R=$C_{18}H_{37}$

In a separate reaction the metalloporphyrins **Zn-(*R*)-6** (50.0 mg, 0.055 mmol) and **Zn-(*R*)-7** (70.0 mg, 0.044) were dissolved in THF (0.018 M) and a solution 1.5 M of KOH was added. The

resulting mixture was stirred overnight at room temperature. The same solution was diluted in water and extracted with $CHCl_3$ and the organic phase was dried over Na_2SO_4 anhydrous and filtrated through cotton wool. The solvent was reduced under pressure to obtain 41.3 mg (83.9%) of the desired acid metalloporphyrin **Zn-(*R*)-12**. After evaporation of the solvent the acid metalloporphyrin **Zn-(*R*)-13** afforded 58.7 mg (84.6%).

5-[4-(*R*)-Methyl-2-phenoxypropanoic acid]-10,15,20-[4-ethoxybenzene] porphyrin zinc (II) Zn-(*R*)-12 : M.F. : $C_{54}H_{46}N_4O_6Zn$; **M.W. :** 898.32 g/mol ; **Found LDI-Tof [M^+] :** 899.1 **^{1}H NMR** (300 MHz, THF-d_8) δ 8.86 (d, *J* = 1.6 Hz, 8H; pyrrole), 8.23-7.89 (m, 8H; ArH), 7.35-7.09 (m, 8H; ArH), 5.06 (d, *J* = 6.9 Hz, 1H; O<u>CH</u>(CH_3)), 4.27 (dt, *J* = 10.2, 5.1 Hz, 6H; O<u>CH_2</u>CH_3), 1.77 (d, *J* = 2.6 Hz, 3H; OCH(<u>CH_3</u>)), 1.67-1.49 (m, 9H; OCH_2<u>CH_3</u>) ; **UV-Vis** ($CHCl_3$) λ_{max}/nm (ε M^{-1} cm^{-1}) : 426 (326067), 554 (12245), 596 (5556).

5-[4-(*R*)-Methyl-2-phenoxypropanoic acid]-10,15,20-[4-octadecaneoxybenzene] porphyrin zinc (II) Zn-(*R*)-13 : M.F. : $C_{101}H_{140}N_4O_6Zn$; **M.W. :** 1571.6 g/mol ; **Found LDI-Tof [M^+] :** 1571.2 ; **^{1}H NMR** (300 MHz, *d*-Chloroform) δ 8.96 (s, 8H; pyrrole), 8.09 (s, 8H; ArH), 7.21 (d, *J* = 9.6 Hz, 8H; ArH), 5.02 (s, 1H; O<u>CH</u>(CH_3)), 4.19 (m, 6H; O<u>CH_2</u>$CH_2(CH_2)_{15}CH_3$), 1.93 (s, 3H; OCH(<u>CH_3</u>)), 1.80-1.51 (m, 6H; OCH_2<u>CH_2</u>$(CH_2)_{15}CH_3$), 1.51-1.12 (m, 90H; OCH_2CH_2(<u>CH_2</u>)$_{15}CH_3$), 1.02-0.74 (m, 9H; $OCH_2CH_2(CH_2)_{15}$<u>CH_3</u>).

3.7.6. Synthesis of the acid chloride porphyrin.

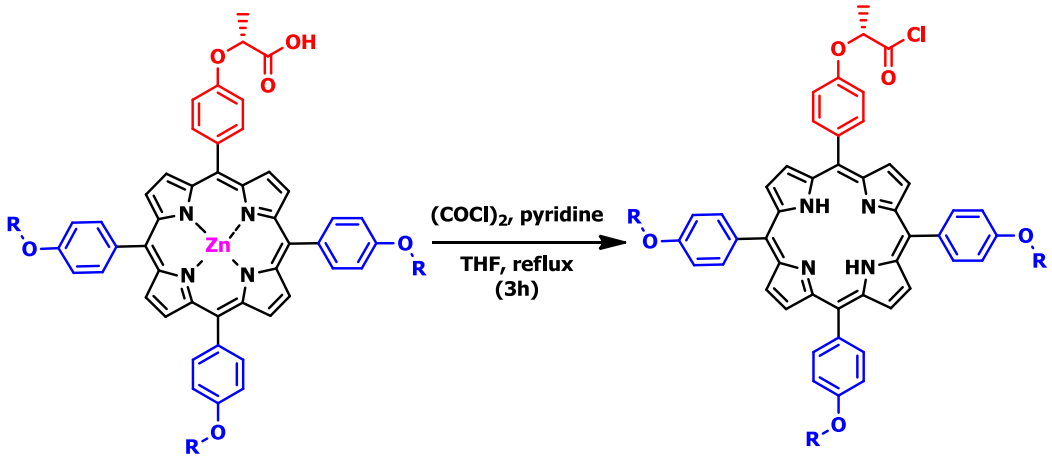

The corresponding chiral acid metalloporphyrin **Zn-(*R*)-12** (78.4 mg, 0.087 mmol) and **Zn-(*R*)-13** (77.0 mg, 0.049 mmol)) was dissolved in dry THF (0.01 M) and stirred under argon atmosphere at 50ºC. Oxalyl chloride (3.0 equivalent) was added dropwise over the solution of the acid metalloporphyrin and immediately a drop of pyridine (10%) was added in the reaction. The

mixture was stirred under inert atmosphere further 3 hours. The solvent was removed under pressure and later under inert atmosphere during 1 hour, the crude compound was used in the next step without further purification.

3.7.7. Coupling between the acid chloride porphyrin intermediate and 3,3'-diamino-2,2'-bipyridine to obtain the porphyrins (*R*)-14 and (*R*)-15.

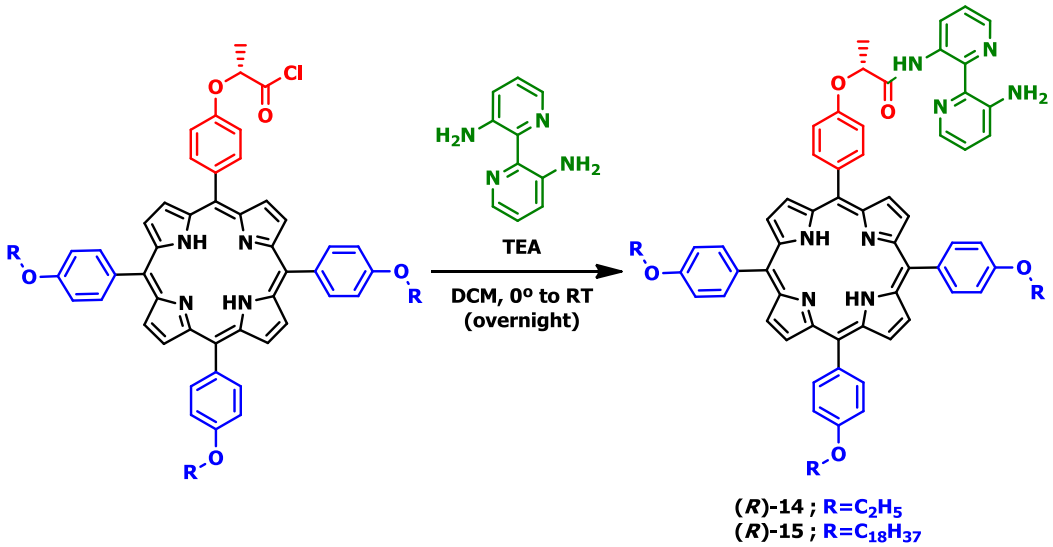

3,3'-diamino-2,2'-bipyridine (1.0 eq.) and TEA (1.1 eq.) were dissolved in dry CH_2Cl_2 (0.05 M) under inert conditions and cold down at 0ºC. A cold solution of the acid chloride intermediate in dry CH_2Cl_2 (0.02 M) was added drop wise over the 3,3'-diamino-2,2'-bipyridine solution. The resulting mixture was stirred from 0ºC (2 hours) to room temperature overnight. The organic layer was extracted with water (x3) and brine (x1) and dried over $MgSO_4$ anhydrous. The solution was filtered through cotton wool and the solvent was removed under pressure. The crude compound was subjected to a silica gel column chromatography (eluent; 1:1 hexane/ CH_2Cl_2 to 7:3 CH_2Cl_2/acetone) to obtain 50.4 mg (57.6 %) of desired porphyrin **(*R*)-14**. For compound **(*R*)-15** 49.3 mg (60.0 %) was obtained as a purple solid.

3'-[5-((4-(*R*)-Methyl-2-phenoxyethoxyl)formylamino)-10,15,20-[4-ethoxybenzene] porphyrin]-2,2'-bipyridine-3-amine (*R*)-14 : M.F. : $C_{63}H_{54}N_8O_5$; **M.W. :** 1003.15 g/mol ; **Found MALDI-Tof [M^+] :** 1002.8 ; **^{1}H NMR** (300 MHz, *d*-Chloroform) δ 14.35 (s, 1H; CONH), 9.12 (d, *J* = 7.1 Hz, 1H; bipy), 8.93-8.81 (m, 8H; pyrrole), 8.33 (d, *J* = 3.1 Hz, 1H; bipy), 8.10 (d, *J* = 8.4 Hz, 4H; ArH), 8.04 (d, *J* = 6.7 Hz, 2H; ArH), 7.98-7.91 (m, 2H; ArH), 7.91-7.84 (m, 2H; bipy), 7.33 (dd, *J* = 8.4, 3.4 Hz, 2H; ArH), 7.26 (m, 4H; ArH), 7.12 (d, *J* = 8.3 Hz, 2H; ArH), 6.95

(m, 2H; bipy), 6.85 (m, 2H; NH_2), 5.05-4.92 (m, 1H; O<u>CH</u>(CH_3)), 4.31 (m, 6H; O<u>CH_2</u>CH_3), 1.87 (d, *J* = 6.7 Hz, 3H; OCH(<u>CH_3</u>)), 1.61 (t, *J* = 7.0 Hz, 9H; OCH_2<u>CH_3</u>), -2.75 (s, 2H; NH) ; **UV-Vis** ($CHCl_3$) λ_{max}/nm (ε M^{-1} cm^{-1}) : 423 (483133), 517 (15077), 555 (15653), 596 (6917), 651 (4117).

3'-[5-((4-(*R*)-Methyl-2-phenoxyethoxyl)formylamino)-10,15,20-[4-octadecaneoxybenzene] porphyrin]-2,2'-bipyridine-3-amine (*R*)-15 : M.F. : $C_{111}H_{150}N_8O_5$; **M.W. :** 1676.4 g/mol ; **Found MALDI-Tof [M^+] :** 1677.5 ; **^{1}H NMR** (300 MHz, *d*-Chloroform) δ 14.35 (s, 1H; CONH), 9.14 (d, *J* = 8.3 Hz, 1H; bipy), 8.88 (s, 6H; pyrrole), 8.77 (s, 2H; pyrrole), 8.34 (s, 1H; bipy), 8.11 (d, *J* = 7.2 Hz, 8H; ArH), 7.34 (d, *J* = 6.7 Hz, 2H; ArH), 7.27 (d, *J* = 7.5 Hz, 6H; ArH), 7.26 (s, 1H; bipy), 7.13 (s, 1H; bipy), 7.05 (d, *J* = 7.8 Hz, 2H; bipy), 6.33 (s, 2H; NH_2), 5.00 (s, 1H; O<u>CH</u>(CH_3)), 4.24 (s, 6H; O<u>CH_2</u>$CH_2(CH_2)_{15}CH_3$), 1.97 (d, *J* = 6.2 Hz, 4H; OCH_2<u>CH_2</u>$(CH_2)_{15}CH_3$), 1.87 (d, *J* = 6.0 Hz, 3H; OCH(<u>CH_3</u>)), 1.60 (d, *J* = 15.7 Hz, 8H; 2H; OCH_2<u>CH_2</u>$(CH_2)_{15}CH_3$, 6H; OCH_2CH_2<u>CH_2</u>$(CH_2)_{14}CH_3$), 1.28 (s, 84H; $OCH_2CH_2CH_2$(<u>CH_2</u>)$_{14}CH_3$), 0.88 (d, *J* = 6.3 Hz, 9H; $OCH_2CH_2(CH_2)_{15}$<u>CH_3</u>), -2.76 (s, 2H; NH).

3.7.8. Metallation of the monoacylated compound (*R*)-15.

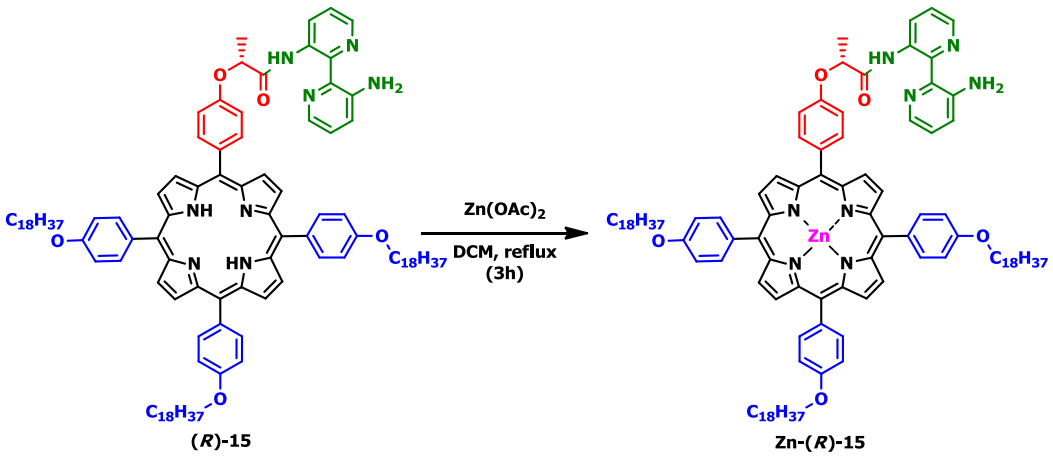

The free-base porphyrin (*R*)-**15** (49.3 mg, 0.03 mmol) was dissolved in CH_2Cl_2 (4.0 ml) and the solution was stirred at reflux under inert atmopehere. $Zn(OAc)_2$ dissolved in 1:1 mixture of CH_2Cl_2/MeOH (0.052 M) was added drop wise with syringe over 5 minutes. The reaction mixture was refluxed further three hours. CH_2Cl_2 was added and the organic layer was washed with a saturated aqueous solution of sodium bicarbonate, brine and was dried over anhydrous Na_2SO_4 and concentrated *in vacuum*. The residue was purified by silica gel chromatography (85:15 ; hexane/DCM) giving 32.5 mg of the desired metalloporphyrin (63.5 %) as a purple metallic powder. **M.F. :** $C_{111}H_{148}N_8O_5Zn$; **M.W. :** 1739.8 g/mol ; **Found MALDI-Tof [M^+] :** 1739.4 ; **^{1}H NMR** (300 MHz, *d*-Chloroform) δ 13.81 (s, 1H; CONH), 8.96 (d, *J* = 16.8 Hz, 6H; pyrrole), 8.82 (s, 2H; pyrrole), 8.13 (d, *J* = 9.9 Hz, 6H; ArH), 8.01 (s, 2H; ArH), 8.01 (s, 1H, bipy), 7.78 (s, 2H;

bipy), 7.30 (s, 8H; ArH), 6.99 (s, 3H; bipy), 6.78 (s, 1H; bipy), 5.87 (s, 2H; bipy), 4.85 (s, 1H; O<u>CH</u>(CH_3)), 4.26 (s, 6H; O<u>CH_2</u>$CH_2(CH_2)_{15}CH_3$), 2.00 (s, 3H; OCH(<u>CH_3</u>)), 1.30 (s, 96H; OCH_2(<u>CH_2</u>)$_{16}CH_3$), 0.92 (s, 9H; $OCH_2CH_2(CH_2)_{15}$<u>CH_3</u>) ; **IR-ATR** (cm^{-1}) : 3416 (bw, NH_2), 2922 (s, CH_2), 2851 (s, CH_2), 1658 (m, CONH), 1604 (m, phenyl), 1506 (m, phenyl), 1237 (s), 992 (s), 800 (s).

3.7.9. Synthesis of the C_3 tris-metalloporphyrin C_3-[Zn-(*R,R,R*)-2].

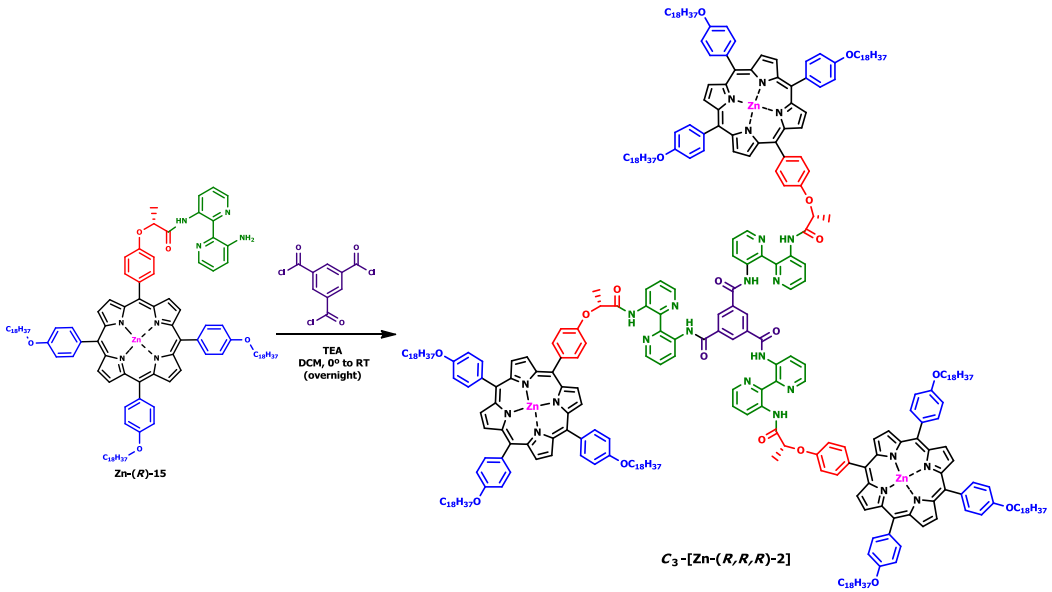

A solution of Zn-(*R*)-**15** (30 mg, 0.017 mmol) and triethylamine (2.65 µl, 0.019 mmol) in 2 ml CH_2Cl_2 was cooled at 0ºC, and then a solution of trimesic chloride (1 µl, $5.6 \cdot 10^{-3}$ mmol) in 0.5 ml CH_2Cl_2 was added dropwise. After 2 hours stirring at 0ºC and one night at room temperature, a purple precipitate was obtained. The solution was filtered and the precipitate washed with dichloromethane, methanol and diethyl ether. After drying, the product was obtained 53.6 mg (58.7%) as a purple powder. **M.F. :** $C_{342}H_{444}N_{24}O_{18}Zn_3$; **M.W. :** 5375.47 g/mol ; **Found MALDI-Tof [M^+] :** 5372.3 ; **^{1}H NMR** (300 MHz, *d*-Chloroform) δ 13.85 (s, CONH), 8.91 (s, pyrrole), 8.78 (s, pyrrole), 8.17 -7.92 (m, ArH), 7.90-7.85 (m, bipy), 7.24 (d, *J* = 11.4 Hz, ArH), 6.98 (s, bipy), 6.85 (d, *J* = 8.7 Hz, bipy), 5.00 (s, O<u>CH</u>(CH_3)), 4.20 (s, O<u>CH_2</u>$CH_2(CH_2)_{15}CH_3$), 1.94 (s, OCH(<u>CH_3</u>)), 1.24 (s, OCH_2(<u>CH_2</u>)$_{16}CH_3$), 0.92-0.79 (m, $OCH_2CH_2(CH_2)_{15}$<u>CH_3</u>).

Chapter 4

Formation of chiral metalloporphyrin-block copolymer complex through metal coordination

4. Formation of chiral metalloporphyrin-block copolymer complex through metal coordination.

4.1. Introduction.

Porphyrins and their derivatives have been widely studied due to their inherent optical and electronic properties that made them suitable for a great variety of applications in nanoelectronic devices,[1] light-harvesting systems[2] or dye-sensitizing.[3] Their electrical and physical properties are easy to tune by the side groups linked in the *meso*-position of the porphyrin ring as well as by the introduction of a metal ion in the core of the chromophore.[4,5]

Free-base porphyrins and metalloporphyrins can self-assemble by different non-covalent interactions such as hydrogen-bonding, π-π interactions or van der Waals, but also the coordination of the metal ion with an exo-facing ligand can drive the self-assembly of the chromophores.[6]

In the last decades, metalloporphyrins have been receiving great attention due to their applications in molecular organic frameworks (MOFs)[7,8] and molecular rotors.[9,10] Specially, the ability of the zinc (II) metal ion to coordinate with nitrogen derivative compounds has opened a broad range of research areas.[11]

On the other hand, a wide variety of polymers have been developed in the recent decades, here we would like to emphasize the so call block copolymers, with different physicochemical properties and therefore suitable in distinct applications, especially in pharmaceutical applications like a drug-delivery systems[12,13] or photodynamic therapy.[14]

(1) Aragonès, A. C.; Darwish, N.; Saletra, W. J.; Pérez-García, L.; Sanz, F.; Puigmartí-Luis, J.; Amabilino, D. B.; Díez-Pérez, I. *Nano Lett.* **2014**, *14*, 4751-4756.
(2) Imahori, H. *J. Phys. Chem. B* **2004**, *108*, 6130-6143.
(3) M'Sabah, B. L.; Boucharef, M.; Warnan, J.; Pellegrin, Y.; Blart, E.; Lucas, B.; Odobel, F.; Bouclé, J. *Phys. Chem. Chem. Phys.* **2015**, *17*, 9910-9918.
(4) Goldberg, I. *Chem. Commun.* ***2005***, 1243-1254.
(5) Chmielewski, P. J.; Latos-Grazynsky, L. *Coord. Chem. Rev.* **2005**, *249*, 2510-2533.
(6) Beletskaya, I.; Tyurin, V. S.; Tsivadze, A. Y.; Guilard, R.; Stern, C. *Chem. Rev.* **2009**, *109*, 1659-1713.
(7) Gao, W-Y.; Chrzanowski, M.; Ma, S. *Chem. Soc. Rev.* **2014**, *43*, 5841-5866.
(8) Wang, K.; Feng, D.; Liu, T-Fu.; Su, J.; Yuan, S.; Chen, Y-P.; Bosch, M.; Zou, X.; Zhou, H-C. *J. Am. Chem. Soc.* **2014**, *136*, 13983-13986.
(9) Puigmartí-Luis, J.; Saletra, W. J. González, A.; Amabilino, D. B.; Pérez-García, L. *Chem. Commun.* **2014**, *50*, 82-84.
(10) Ogi, S.; Ikeda, T.; Wakabayashi, R.; Shinkai, S.; Takeuchi, M. *Chem. Eur. J.* **2010**, *16*, 8285-8290.
(11) Sguerra, F.; Bulach, V.; Hosseini, M. W. *Dalton Trans.* **2012**, *41*, 14683-14689.
(12) Leggins, R. T.; Burt, H. M. *Adv. Drug. Deliv. Rev.* **2002**, *54*, 191-202.
(13) Bronich, T. K.; Vinogradov, S. V.; Kabanov, A. V. *Nano. Lett.* **2001**, *1*, 535-540.
(14) Bo, Q.; Zhao, Y. J. *Polym. Sci. Pol. Chem.* **2006**, *44*, 1734-1744.

The block copolymers are a class of polymers formed by two or more distinct polymer fragments linked by covalent bonds. The simplest block copolymers are made by two different block polymerized monomers A and B (linear diblock copolymer).[15] An example of block copolymer of polystyrene-*b*-polyisoprene is shown in Figure 1.

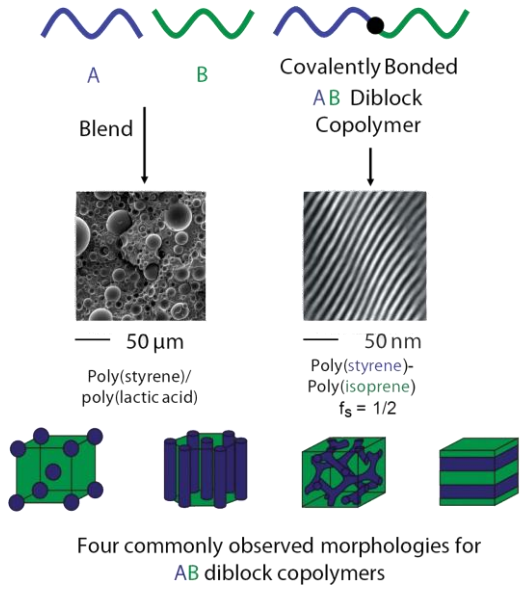

Figure 1. Illustration of AB diblock copolymers.

Commonly, they are prepared by a living polymerization of two different types of monomers,[16] typically one hydrophobic and another part hydrophilic, providing as a result amphiphilic polymers composed by two differentiate regions with different affinity to the solvents,[17] factor that evolves into different morphologies due to phase segregation.[18]

The study of block copolymers with a head reactive group, in one of the blocks, might the possibility to functionalize the polymer via non-covalent interactions affording supramolecular structures suitable for applications in different fields.[19,20] This is the case of block copolymers which structure is composed by a poly(vinyl pyridine) block due to its ability to coordinate with Lewis acids,[21] such as Poly(styrene-*b*-4-vinyl pyridine) (PS-*b*-P4VP) block copolymer, that is a

(15) Alexandridis, P. *Curr. Opin. Colloid. In.* **1996**, *1*, 490-501.
(16) Hadjichristidis, N.; Iatrou, H.; Pitsikalis, M.; Mays, J. *Prog. Polym. Sci.* **2006**, *31*, 1068-1132.
(17) Letchford, K.; Burt, H. *Eur. J. Pharm. Biopharm.* **2007**, *65*, 259-269.
(18) Matsen, M. W.; Bates, F. S. *J. Chem. Phys.* **1997**, *106*, 2436-2448.
(19) Stupp, S. I.; Palmer, L. C. *Chem. Mater.* **2014**, *26*, 507-518.
(20) Li, J.; An, Y.; Chen, X.; Xiang, D.; Li, Y.; Huang, N.; Shi, L. *Macromol. Rapid Commun.* **2008**, *29*, 214-218.
(21) Bronstein, L. M.; Sidorov, S. N.; Valetsky, P. M. *Langmuir* **1999**, *15*, 6256-6262.

versatile organic polymer due to its amphiphilic character and can easily functionalize through the pyridine unit.[22,23]

4.2. Objectives.

The objective of this project is:

The construction of chiral dye-polymers via axial metal coordination for potential applications in optoelectronic devices.

The project will be focused in the specific objectives:

- Prepare chiral functional molecules derived from metalloporphyrins.
- Determine the chirality transfer in the supramolecular organization of the Poly(styrene-*b*-4-vinyl pyridine) (PS-*b*-P4VP) block copolymer.

The chiral zinc (II) metalloporphyrin Zn-(*R,R,R,R*)-**1** has been synthesized as a dye unit following a common route. The four lactatamide groups in the *meso*-positions, provide the chiral centers while the long alkyl chains improve the overall solubility of the final molecule.

For this purpose, Poly(styrene-*b*-4-vinyl pyridine) block copolymer has been used as a polymeric matrix due to the 4-vinyl pyridine unit that acts as an anchoring side for the zinc (II) ion of the metalloporphyrin ring (Figure 2).[24]

(22) Guldi, D. M.; Rahman, G. M. A.; Quin, S.; Tchoul, M.; Ford, W. T.; Marcaccio, M.; Paolucci, D.; Paolucci, F.; Campidelli, S.; Prato, M. *Chem. Eur. J.* **2006**, *12*, 2152-2161.
(23) Arulkashmir, A.; Mahale, R. Y.; Dharmapurikar, S. S.; Jangid, M. K.; Krishnamoorthy, K. *Polym. Chem.* **2012**, *3*, 1641-1646.
(24) Priimagi, A.; Cattaneo, S.; Ras, R. H. A.; Valkama, S.; Ikkala, O.; Kauranen, M. *Chem. Mater.* **2005**, *17*, 5798-5802.

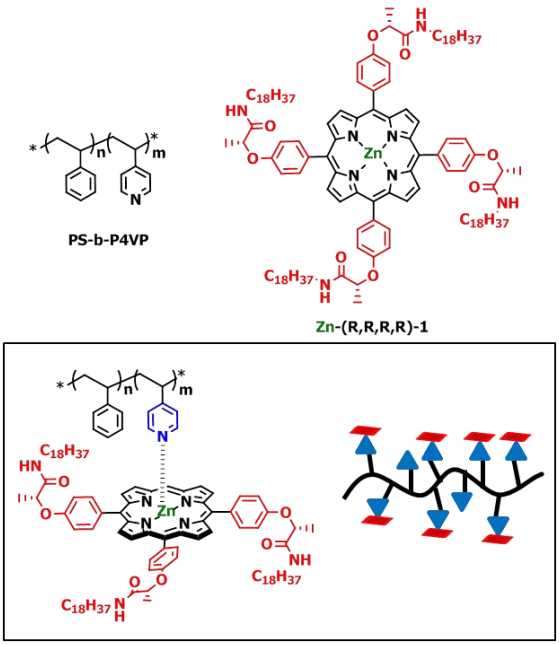

Figure 2. Illustration of the supramolecular organization of the [Zn-(*R,R,R,R*)-**1**]-BCP complex**.**

The coordination studies and the supramolecular organization has been performed in solution by UV-Vis absorption spectroscopy, fluorescence and circular dichroism spectroscopy (CD, a chiroptical tool that allows precise monitoring of aggregation) to obtain information about the complex architecture and relative orientations of molecules inside aggregates.[25]

4.3. Synthesis of the chiral metalloporphyrins and its achiral homologous.

4.3.1. Synthesis of the chiral metalloporphyrins Zn-(*R,R,R,R*)-3 and Zn-(*R,R,R,R*)-1.

The chiral metalloporphyrin under study contains four chiral amide groups in the *meso*-positions of the porphyrin ring and was synthesized following a short synthetic route (Scheme 1).

(25) Pescitelli, G.; Di Bari, L.; Berova, N. *Chem. Soc. Rev.* **2014**, *43*, 5211-5233.

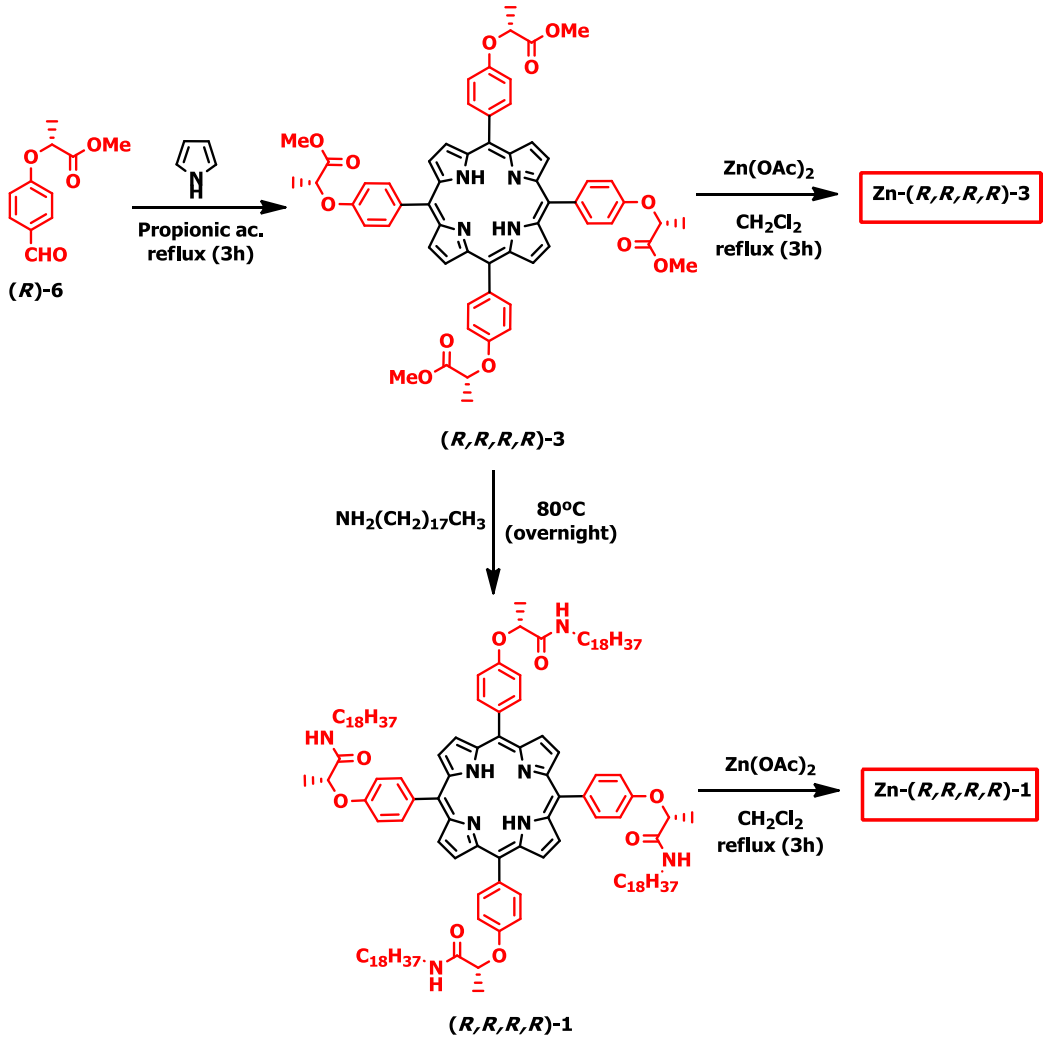

Scheme 1. Synthesis of chiral test metalloporphyrin Zn-(*R,R,R,R*)-**3** and the desired chiral metalloporphyrin Zn-(*R,R,R,R*)-**1**.

The first step, before to construct the porphyrin ring, involved the synthesize of the chiral lactate aldehyde derivative (*R*)-**6** by the use of the Mitsunobu reaction.[26,27,28]

The condensation of the aldehyde (*R*)-**6** with pyrrole in a 1:1 mixture using the Adler and Longo method afforded the chiral porphyrin (*R,R,R,R*)-**3**.[29] It is worthy to note, that as the porphyrin is symmetric, the purification process was easily handled achieving the porphyrin in pure

(26) Minguet, M.; Amabilino, D. B.; Vidal-Gancedo, J.; Wurst, K.; Veciana, J. *J. Mater. Chem.* **2002**, *12*, 570-578.
(27) Ahn, C.; Correia, R.; DeShong, P. *J. Org. Chem.* **2002**, *67*, 1751-1753.
(28) This step has been explained in detail in **Chapter 2**.
(29) Linares, M.; Iavicoli, P.; Psychogyiopoulou, K.; Beljonne, D.; De Feyter, S.; Amabilino, D. B.; Lazzaroni, R. *Langmuir* **2008**, *24*, 9566-9574.

form.[30] Even though the yield obtained for the chiral porphyrin was not overcoming 6 %. We have to keep in mind that the yields obtained in these conditions, usually rarely exceeded 20 %,[31] the low yield could be attributed to the low reactivity of the chiral aldehyde and therefore the non consumption of all the starting materials during the reaction time, as could be demonstrated after the silica gel column chromatography.

The chiral porphyrin (*R,R,R,R*)-**1** was prepared by the reaction of the chiral lactate porphyrin (*R,R,R,R*)-**3** with an excess of the octadecylamine at 80ºC (overnight), using the later as a reactant and as solvent due to the lower melting point of the amine (~ 50 ºC).[32] The amidation reaction afforded in a 76 % yield the desired free-base porphyrin (*R,R,R,R*)-**1** after purification by column chromatography and exclusion chromatography (in order to remove completely the excess of octadecylamine).

The ^{1}H-NMR of the chiral amide porphyrin (*R,R,R,R*)-**1** revealed the formation of the desired compound. Figure 3 shows the comparison of the starting free-base porphyrin (*R,R,R,R*)-**3** and the final chiral amide porphyrin, (*R,R,R,R*)-**1**.

As the spectra shows, the amide proton appeared as a triplet at 6.69 ppm. Moreover, in the upper field region it can be appreciated the protons related to the long alkyl chain and the disappearance of the singlet of the ester protons at around 4.00 ppm, fact that corroborated the success of the reaction.

(30) The synthesis of porphyrins has been explained in more detail in the general introduction (***Chapter 1***).
(31) Sun, Z-C.; She, Y-B.; Zhoa, Y.; Song, X-F.; Li, K. *Molecules* **2011**, *16*, 2960-2970.
(32) Iavicoli, P.; Xu, H.; Feldborg, L. N.; Linares, M.; Paradinas, M.; Stafström, S.; Ocal, C.; Nieto-Ortega, B.; Casado, J.; López Navarrete, J. T.; Lazzaroni, R.; De Feyter, S.; Amabilino, D. B. *J. Am. Chem. Soc.* **2010**, *132*, 9350-9362.

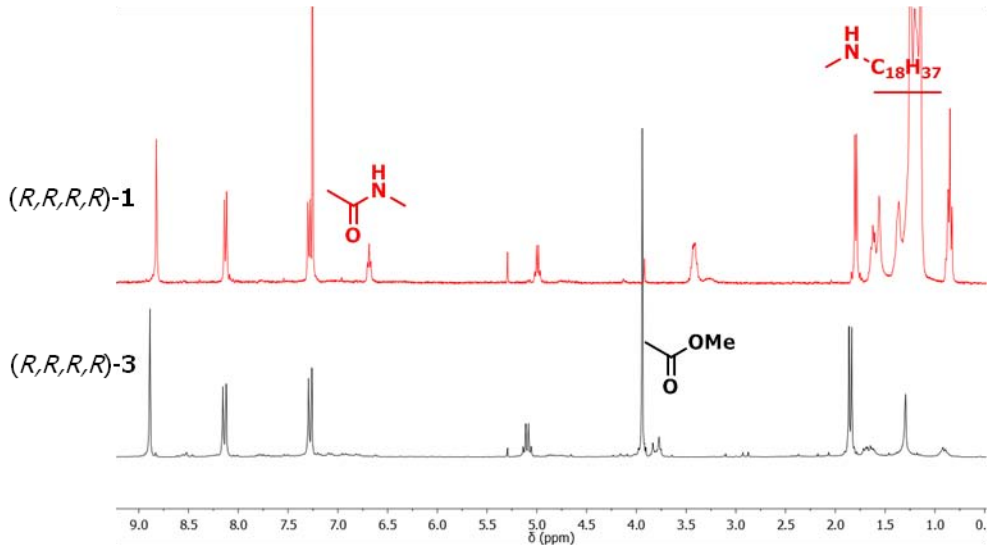

Figure 3. Comparison of ^{1}H-NMR of free-base porphyrin (*R,R,R,R*)-**3** and (*R,R,R,R*)-**1** in $CDCl_3$.

The insertion of the metal ion in the core of the porphyrin ring was by means of the utilization of the zinc acetate salt.[33] The two free-base porphyrins, (*R,R,R,R*)-**3** and (*R,R,R,R*)-**1,** were reacted with the metal salt in mild conditions to afford, after a process of fast purification, approximately 70 % yield of the chiral lactate metalloporphyrin Zn-(*R,R,R,R*)-**3** and chiral amide metalloporphyrin Zn-(*R,R,R,R*)-**1**, respectively (Figure 4).

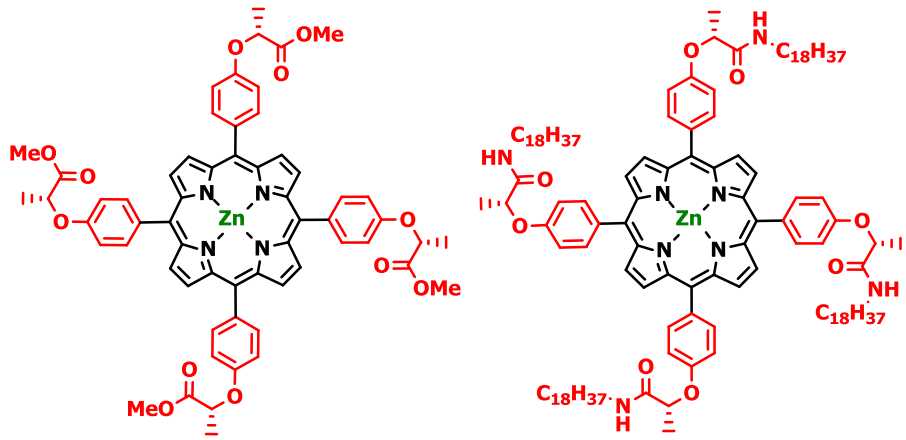

Figure 4. Structure of the metalloporphyrins Zn-(*R,R,R,R*)-**3 and** Zn-(*R,R,R,R*)-**1.**

(33) Feldborg, L. N.; Saletra, W. J.; Iavicoli, P.; Amabilino, D. B. *J. Porphyr. Phthalocya.* **2011**, *15*, 995-1003.

4.3.2. Synthesis of the achiral metalloporphyrin Zn-2.

In this work, the chirality transfer from a chiral metalloporphyrin to a diblock copolymer has been studied. In order to compare the results, the achiral homologue of the metalloporphyrin Zn-(*R,R,R,R*)-**1** has been synthesized to observe the influence of the chiral groups in the side chains of the metalloporphyrin in the supramolecular organization of the complex.

For this purpose the achiral metalloporphyrin Zn-**2** was prepared as shown in Scheme 2.

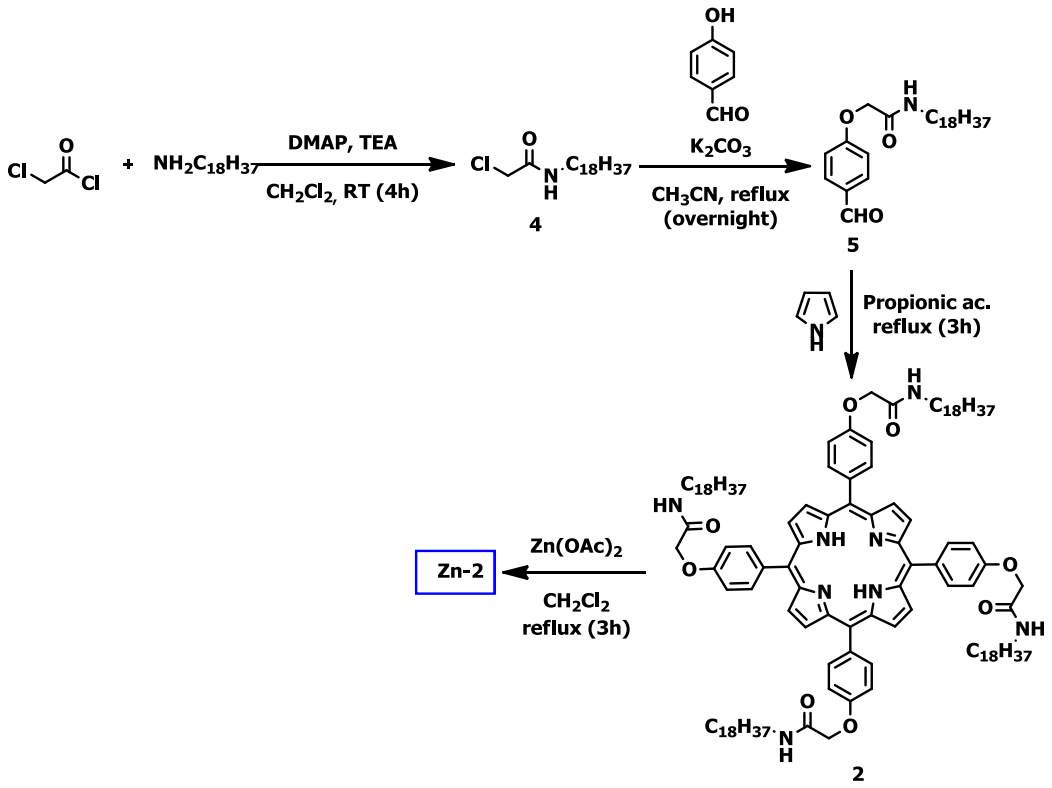

Scheme 2. Synthesis of the desired achiral metalloporphyrin Zn-**2**.

The first step of the synthesis was the reaction between a primary amine with an acid chloride to form the corresponding amide compound **4**. In this process acid chloride is formed, that's why a base is needed in the reaction in order to neutralize the acid (Scheme 3).[34]

(34) Montalbetti, C. A. G. N.; Falque, V. *Tetrahedron* **2005**, *61*, 10827-10852.

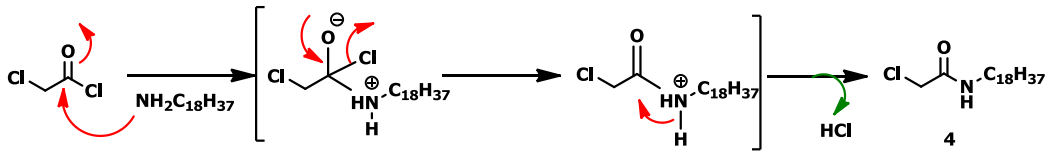

Scheme 3. Mechanism of the formation of the amide **4**.

The second step is the nucleophilic attack (S_N2)[35] of the 4-hydroxybenzaldehyde to the amide compound **4** to obtain the amide aldehydes **5** that will be used in the following step to form the free-base porphyrin **2**.

As explained above, the synthesis of the porphyrin ring was following the Adler and Longo method, affording after purification 8 % yield of the desired free-base porphyrin.

When the ^{1}H-NMR spectrum of the achiral porphyrin **2** was compared with the spectrum of the chiral porphyrin (*R,R,R,R*)-**1**, slightly differences were observed (Figure 5).

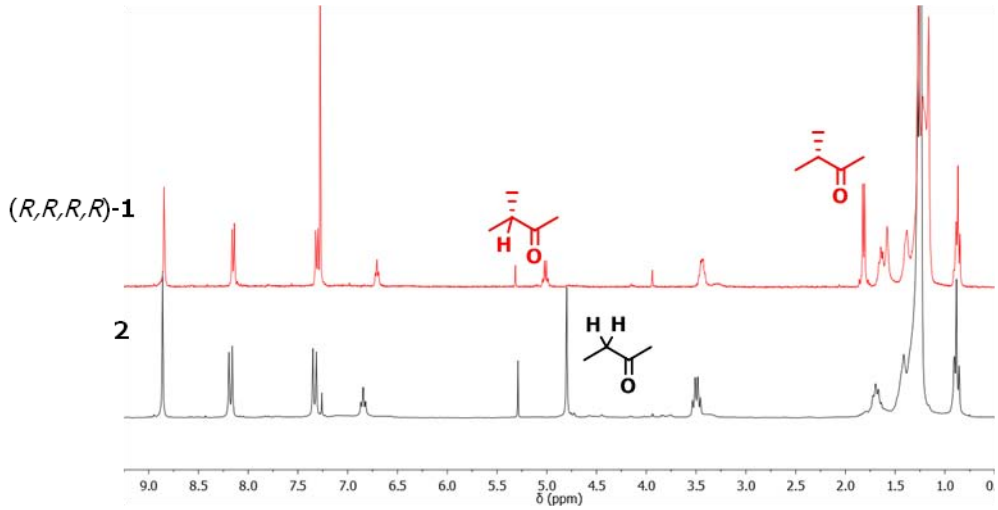

Figure 5. Comparison of ^{1}H-NMR of free-base porphyrin **2** and (*R,R,R,R*)-**1** in $CDCl_3$.

As it was expected, the main differences observes when the both spectra when they were compared, appear in the protons of the chiral center. In the case of the chiral porphyrin, (*R,R,R,R*)-**1,** appeared a quadruplet at 5.00 ppm corresponding to the chiral proton (next to the amide group) as well as a doublet at around 1.90 ppm that was assigned to the methyl group bonded in the stereogenic center. However, porphyrin **2** presented a singlet peak at around 4.75 ppm that was attributed to the CH_2 between the phenoxy and the amide groups.

(35) This step has been explained in detail in ***Chapter 3***.

The same procedure than before was used to introduce the zinc (II) metal ion in the core of the chromophore ring. The free-base porphyrin **2** was reacted with the metal salt in dichloromethane under inert conditions. After be purified by a fast column chromatography the desired metalloporphyrin Zn-**2** was obtained in a good yield as a purple solid (Figure 6).

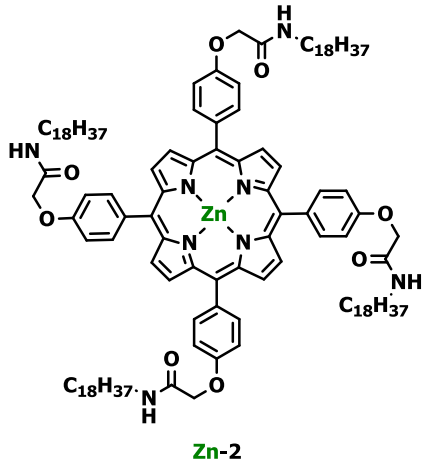

Figure 6. Structure of the metalloporphyrin Zn-**2**.

4.3.3. Synthesis of the block copolymer PS-*b*-P4VP (BCP).

The block copolymer PS-*b*-P4VP (molar ratio PS:P4VP 1:4) was previously synthesized by living anionic polymerization following the methodology described by Varshney et al.[36] This work was performed by a PhD student of the group, as the topic is in collaboration with.

4.4. Supramolecular organization of metalloporphyrin-BCP complex in solution.

4.4.1. Titration studies of the porphyrin reference Zn-(*R,R,R,R*)-3.

A titration study of the lactate metalloporphyrin derivative Zn-(*R,R,R,R*)-**3** with pyridine to form [Zn-(*R,R,R,R*)-**3**-Py] (Figure 7) was followed by UV-Visible absorption spectroscopy.[37] This study was performed as a reference to compare lately with further experiments because as it is well known, the coordination of the metal ion with a pyridine group as always implies a red-shift of the absorption bands in the spectra; therefore, the results observed for the metalloporphyrin test can be extrapolated to the changes in the UV-Visible spectrum of the metalloporphyrins under study, due to structural similarities.

(36) Varshney, S. K.; Zhong, X. F.; Eisenberg, A. *Macromolecules* **1993**, *26*, 701-706.
(37) Fleischer, E. B.; Shachter, A. M. *Inorg. Chem.* **1991**, *30*, 3763-3769.

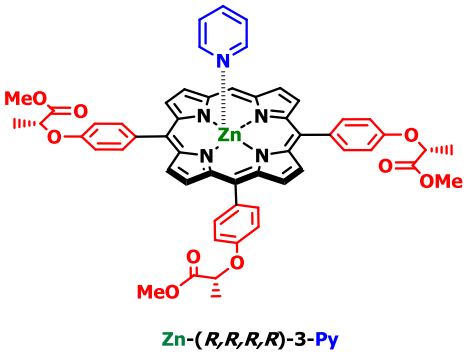

Figure 7. Coordination of Zn-(*R,R,R,R*)-**3** with pyridine through the zinc (II) metal ion.

Zinc (II) porphyrins tend to bind with nitrogen axial ligands and as a result, a red shift of the absorption bands appears due to an increase of the electron density of the porphyrin ring.[33]

The experiment was carried out at room temperature in dichloromethane at concentration 5 μM of the metalloporphyrin (Sol. A) and consecutive additions of pyridine solution up to 1.5 mM, in which the total coordination of the ligand was observed (Figure 8). In order to maintained the concentration constant of the metalloporphyrin Zn-(*R,R,R,R*)-**3** during the titration studies, pyridine (1.5 mM) was mixed with a 5 μM solution of the metalloporphyrin under study (Sol.B).

As it can observed in the UV-Visible absorption spectra, solution A, that correspond the initial metalloporphyrin solution, presented at 423 nm a maximum for the Soret band of the isolated compound and two Q-bands at 550 nm and 590 nm. As the concentration of pyridine increase in the solution, the relative intensity for the Soret band decreased progressively as well as the higher energy Q-band (Q_α), while the lower energy Q-band (Q_β) experienced an increasing of the relative intensity.

An important shift of the absorption bands to lower energies was evidenced after the addition of 0.15 mM of pyridine,. A clear bathochromic shift of the Soret band from 423 nm to 430 nm was observed. The shift of the Q_α band was from 550 nm to 564 nm and, for the lower energy Q-band (Q_β) the shift was from 590 to 605 nm. Moreover Q_β showed a clear increase in the relative intensity as the pyridine content rise up to 0.15 mM.[38] These results clearly indicate the coordination of one pyridine unit with the zinc (II) metal ion to form the pentacoordinated metalloporphyrin.[39]

(38) Gautam, R.; Chauan, S. M. S. *Mat. Sci. Eng. C* **2014**, *43*, 447–457.
(39) Alessio, E. (Ed.), *Structure and Bonds : Non-covalent multi-porphyrin assemblies synthesis and properties*, Springer, *121*, 1-47, **2006**.

Figure 8. Titration of Zn-(*R,R,R,R*)-**3** (5 μM) with pyridine.

4.4.2. Titration studies of the achiral metalloporphyrin Zn-2.

Towards the complexation of BCP with the metalloporphyrin, a PS-*b*-P4VP and the achiral Zn (II) porphyrin Zn-**2** were employed ([Zn-**2**]-BCP) (Figure 9).

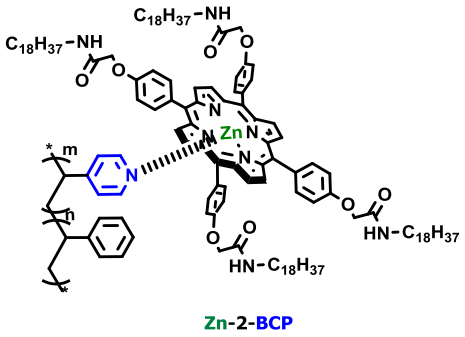

Figure 9. Schematic representation of the [Zn-**2**]-BCP complex.

Additionally to the coordination between the pyridine groups of the PS-*b*-P4VP and zinc (II) metal ion in the core of the porphyrin, Zn-**2** can self-assemble by the coordination of the carbonyl group of the amide in the periphery with the zinc of an adjacent metalloporphyrin. However, the conditions used in the titration studies did not favor the self-aggregation of the metalloporphyrin to focus exclusively on the effects of the coordination among prophyrins and the block copolymer.

The formation of the complex was followed by UV-Visible absorption in chloroform, solvent that kept porphyrin as isolated monomer in solution, avoiding the self-aggregation of the metalloporphyrin due to the non-coordinating character of the solvent. Thus, ensured that changes, appreciated in the UV-Visible absorption spectra as the result of the addition of PS-*b*-P4VP, would rely on the coordination between the polyvinyl pyridine units and the metalloporphyrin.

For this, a 50 μM of Zn-**2** solution in chloroform was prepared (Sol. A). Concurrently, in order to keep the concentration of the metalloporphyrin constant respect to the PS-*b*-P4VP during the analysis, another mixed solution composed by 47 μM of Zn-**2** and 0.5 mM of PS-*b*-P4VP as well in chloroform was prepared (Sol. B). The UV-Visible absorption analysis started with the measurement of the absorption of the metalloporphyrin solution (Sol. A), and amounts of Sol. B were repeatedly added to it meanwhile the changes were tracked (Figure 10).[40]

Figure 10. Titration of Zn-**2** (47 μM) with BCP.

The UV-Visible absorption spectra of [Zn-**2**]-BCP (Figure 10) shows the progressive evolution of the Q-bands while increasing the concentration of BCP in the final solution. The absorption band corresponding to the Q_α band of the isolated metallocompound Zn-**2** was found at 556 nm, which increased in intensity and shifted to 564 nm as the concentration of PS-*b*-P4VP increased in the solution. In the case of the Q_β band experienced a bathochromic shift from 598 nm to 605 nm due to the increasing concentration of the PS-*b*-P4VP in the working solution. As mentioned above, the relative concentration of the metalloporphyrin in the quartz cuvette was kept constant, so the observed changes could be directly related with the coupling between the block copolymer and the metalloporphyrin through the coordination of zinc (II) metal ion with the pyridyl unit of the polymer towards the formation of the [Zn-**2**]-BCP complex.[41]

Moreover, a clear isosbestic point was observed at 544 nm and a second isosbestic point at 591 nm less evidence than the previous one, that suggested the equilibrium between two different species in solution, the isolated metalloporphyrin and the [Zn-**2**]-BCP complex.

(40) Gao, B.; Wang, R.; Du, R. *J. Porphyr. Phthalocya.* **2010**, *14*, 235-243.
(41) Ikeda, C.; Fujiwara, E.; Satake, A.; Kobuke, Y. *Chem. Commun.* **2003**, 616-617.

4.4.3. Coordination studies of the chiral metalloporphyrin Zn-(*R,R,R,R*)-1 with BCP.

One of the most noticeable and appreciated characteristics of the Zn (II) porphyrins is their capability to self-assemble through their metallic core. In a previous work it was observed that metalloporphyrin Zn-(*R,R,R,R*)-**1** self-assembled in non-polar solvents through the coordination between the carbonyl group of the amide and the zinc (II) metal ion of an adjacent porphyrin forming dimer aggregates.**iError! Marcador no definido.** The coordination studies between the block copolymer PS-*b*-P4VP and the chiral metalloporphyrin Zn-(*R,R,R,R*)-**1** might allow the chiral amplification in the supramolecular structure [Zn-(*R,R,R,R*)-**1**]-BCP formed by sergeant and soldier effects (Figure 11).[42,43]

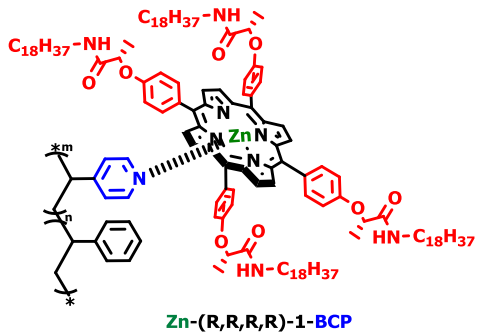

Figure 11. Schematic representation of the [Zn-(*R,R,R,R*)-**1**]-BCP complex.

4.4.3.1. Titration studies of the chiral metalloporphyrin Zn-(*R,R,R,R*)-1.

The titration of the metalloporphyrin Zn-(*R,R,R,R*)-**1** with the PS-*b*-P4VP block copolymer was followed by UV-Visible absorption spectroscopy, following the same conditions applied for its achiral homologue. A 50 μM solution of Zn-(*R,R,R,R*)-**1** in chloroform was prepared (Sol. A). Concurrently, in order to keep the concentration of the metalloporphyrin constant respect to the PS-*b*-P4VP during the titration process, another mixed solution formed by 50 μM of Zn-(*R,R,R,R*)-**1** and 0.5 mM of PS-*b*-P4VP also in chloroform was prepared (Sol. B).

Figure 12 shows the progressive evolution of the Q-bands of the metalloporphyrin Zn-(*R,R,R,R*)-**1** in increasing the BCP concentration in the working solution. This behavior is un concordance with the analogous achiral Zn-**2** and also with the reference test titration of the Zn-(*R,R,R,R*)-**3** with pyridine. Q_β band shifted at higher wavelengths, as in the other systems was

(42) Green, M. M.; Reidy, M. P. *J. Am. Chem. Soc.* **1989**, *111*, 6452-6454.
(43) Anderson, T. W.; Sanders, J. K. M.; Pantos, G. D. *Org. Biomol. Chem.* **2010**, *8*, 4274-4280.

observed, and its relative intensity increased progressively as the metalloporphyrin was coordinated with the pyridyl unit of the PS-*b*-P4VP. However, a differentiated behavior was noticed in the evolution of Q_α band compared with the titration of the achiral metalloporphyrin, where now a red shift of this band could be spotted.

Figure 12. Titration of Zn-(*R,R,R,R*)-**1** (50 μM) with BCP.

In order to observe clearly the evolution of the isolated metalloporphyrin towards the formation of the [Zn-(*R,R,R,R*)-**1**]-BCP complex, in the UV-Visible absorption spectra only some curves at different concentration of BCP in the working solution are presented (Figure 13).

As observed in the spectra, the isolated metalloporphyrin Zn-(*R,R,R,R*)-**1** showed two maximum absorptions at 555 nm and at 597 nm, for the Q_α and Q_β bands respectively. Firstly, at low concentrations of BCP in the porphyrinic solution, Q_α band experienced a slight decrease of the relative intensity and afterwards, while increasing the concentration of the BCP, Q_α band slightly increases and moves to higher wavelength since to 563 nm, position of Q_α band in solution B. In the case of the lower energy Q-band (Q_β) a progressive red-shift and a gradual increment was noticed since achieved a maximum in solution B at 606 nm, where the concentration of BCP was 0.5 mM, meaning that all the metallporphyirin present in the solution is coordinated with a pyridyl unit of the block compolymer.

Moreover, the presence of two isosbestic points at 534 nm and at 588 nm in the absorption spectra indicated the equilibrium between monomer Zn-(*R,R,R,R*)-**1** metalloporphyrin and the complex [Zn-(*R,R,R,R*)-**1**]-BCP formed by the coordination through the metal ion.[44]

(44) Cai, Y-Q.; Ren, X-B.; Wang, H-L.; Huang, H-X.; Chen, M.; Qian, D-J. *Synthetic Met.* **2012**, *162*, 1871-1878.

Figure 13. Titration of Zn-(*R,R,R,R*)-**1** (50 μM) with BCP.

The coordination process for the chiral system slightly differed from the formation of the achiral [Zn-**2**]-BCP complex; evidences of such fact are seen by following the evolution of the Q_α band. Such variations could be attributed to the steric hindrance due to the chiral methyl groups in the lateral chains that slowed down the coordination between the pyridyl unit and the zinc (II) metal ion.

4.4.3.2. Fluorescence studies of the [Zn-(*R,R,R,R*)-1]-BCP complex.

On the other hand, complementary to the UV-Visible absorption studies, fluorescence spectroscopic measurements were performed for the chiral metalloporphyrin Zn-(*R,R,R,R*)-**1** and its complex [Zn-(*R,R,R,R*)-**1**]-BCP (Figure 14). For this, solutions 5 μM of Zn-(*R,R,R,R*)-**1** and 5 μM of [Zn-(*R,R,R,R*)-**1**]-BCP in chloroform were prepared.

Figure 14 shows the emission from the first excited state (S_1) to the ground state (S_0) upon excitation at 551 nm and 601 nm in metalloporphyrin Zn-(*R,R,R,R*)-**1** and 554 nm and 601 nm in the complex [Zn-(*R,R,R,R*)-**1**]-BCP. The emission spectrum of the [Zn-(*R,R,R,R*)-**1**]-BCP complex (Figure 14) was red-shifted compared with the emission spectrum of the isolated metalloporphyrin Zn-(*R,R,R,R*)-**1**, according what it was observed in the UV-Visible absorption studies. These results suggested that the fluorescence properties of the metalloporphyrin were not altered by the electron density gain of the porphyrin ring when it was coordinated by the pyridyl moiety of the BCP.

However, the Q_β-band presented a larger stock shift (62 nm) for the [Zn-(*R,R,R,R*)-**1**]-BCP respect to the Zn-(*R,R,R,R*)-**1** (55 nm), probably due to the electron-donator character of the pyridyl group.[45,46]

Figure 14. UV-Visible absorption and fluorescence spectra of Zn-(*R,R,R,R*)-**1** (5 μM) and [Zn-(*R,R,R,R*)-**1**]-BCP complex (5 μM).

4.4.3.3. CD studies of the [Zn-(R,R,R,R)-1]-BCP complex.

Seizing upon the chirality of the Zn-(*R,R,R,R*)-**1**, circular dichroism spectroscopy (CD) was a suitable complementary spectroscopic technique because its sensitive to supramolecular structures, absolute configurations and features that are not straightforward to be detected in other spectroscopic techniques. The CD principle is based in the absorption difference of the left- and right-handed polarized light and, the CD signal intensity and position might be affected by the perturbation in the surroundings of the chromophore.[47] In this way, 50 μM solution of Zn-(*R,R,R,R*)-**1** and 50 μM solution of PS-*b*-P4VP both in chloroform, were mixed together to obtain a 5 μM solution of [Zn-(*R,R,R,R*)-**1**]-BCP complex and then, the mixture was analyzed within the temperature range 0 °C to 60 °C (Figure 15).

The CD spectra showed a slight temperature-dependence behavior of [Zn-(*R,R,R,R*)-**1**]-BCP complex, being more evidence in the Q-bands in the corresponding absorption spectra. As the temperature increased, a slight blue-shift was observed, suggesting a possible decoordination between the pyridyl unit of the BCP and the zinc (II) metal ion of the porphyrin. The evolution of the CD signal suggested a chiral organization of the [Zn-(*R,R,R,R*)-**1**]-BCP complex with a

(45) Apanasovich, V. V.; Novikov, E. G.; Yatskov, N. N.; Koehorst, R. B. M.; Schaafsma, T. J.; van Hoek, A. *J. Appl. Spectrosc.* **1999**, *66*, 613-616.
(46) Karolezak, J.; Kowalska, D.; Lukaszewicz, A.; Maciejewski, A.; Steer, R. P. *J. Phys. Chem. A* **2004**, *108*, 4570-4575.
(47) Gottarelli, G.; Lena, S.; Masiero, S.; Pieraccini, S.; Spada, G. P. *Chirality* **2008**, *20*, 471-485.

preferential absorption of the left- or right-handed polarized light transferred from the chirality of the Zn-(*R,R,R,R*)-**1** to the complex. Moreover, the absence of Cotton effect in the CD spectrum indicated that the CD signals were from the [Zn-(*R,R,R,R*)-**1**]-BCP complex instead of the chromophore-chromophore interactions. These results were in concordance with the ones observed in the titration studies.[48]

Figure 15. CD and the corresponding absorption spectra of the [Zn-(*R,R,R,R*)-**1**]-BCP complex (5 μM) within the temperature range 0ºC to 60ºC.

Figure 16 shows the propose chiral superstructure that the [Zn-(*R,R,R,R*)-**1**]-BCP complex may form in solution, based on the optical activity observed in the CD studies.

(48) Pale, V.; Nikkonen, T.; Vapaavuori, J.; Kostiainen, M.; Kavakka, J.; Selin, J.; Tittonen, I.; Helaja, J. *J. Mater. Chem. C.* **2013**, *1*, 2166-2173.

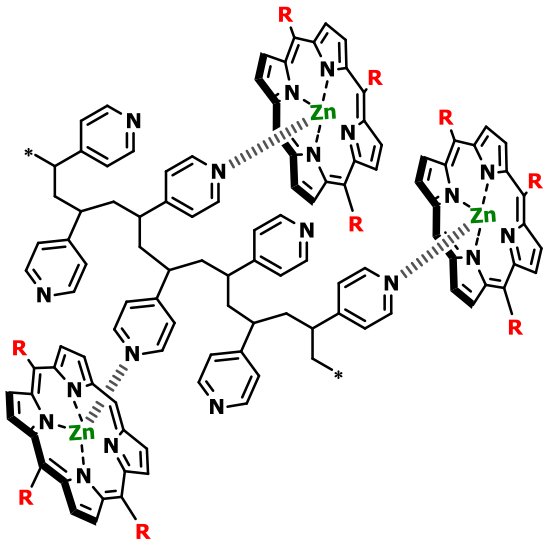

Figure 16. Illustration of Zn-Pyridine interaction in the [Zn-(*R,R,R,R*)-**1**]-BCP complex.

4.5. Supramolecular organization of metalloporphyrin-BCP complex on surface.

As this topic was in collaboration with another PhD member of the group, the results obtained about the morphology organization on surface of the achiral complex [Zn-**2**]-BCP and the analogous chiral complex [Zn-(*R,R,R,R*)-**1**]-BCP are explained in detail in her thesis manuscript.

However, a brief description of these analyses is explained in this part.

UV-Visible absorption spectroscopy on slide quartz surface were analyzed for the metalloporphyrin-BCP complexes in order to see if any variation could be observed respect to the results obtained in solution, and to be consistent with further morphology studies by atomic force microscopy (AFM) in HOPG surface, scanning electron microscopy (SEM) and transmission electron microscopy (TEM).

The UV-Visible absorption analyses revealed that the coordination was maintained after several drops of complex solution were deposited on the quartz surface.

Nevertheless, none of the microscopy analyses showed any evidence of chirality transfer in the morphology of the [Zn-(*R,R,R,R*)-**1**]-BCP complex, even though such experiments are bee carefully studied at present.

4.6. Conclusions.

It has been demonstrate the ability of the zinc (II) metal ion to coordinate with nitrogen compounds derivative. Precisely, the titration studies of the achiral metalloporphyrin Zn-**2** and its

homologous chiral metalloporphyrin Zn-(*R,R,R,R*)-**1** demonstrate the formation of a complex with the block copolymer through the coordination of the pyridyl unit with the zinc (II) metal ion in the core of the porphyrin ring.

It has been observed that the chiral groups in the lateral chains did not affect in the coordination process and the evolution of the Q-bands followed by UV-Visible absorption spectroscopy presented similar tendency as the concentration of the BCP increased in the working solution.

Moreover, the CD studies performed for the chiral complex showed poor chirality transfer from the porphyrin ring to the supramolecular architecture, scorning that the optical activity observed was coming from the interaction among chromophores due to the fact that no Cotton effect was observed, typically from the electronic transitions between porphyrin units.

4.7. Experimental section.

NMR spectra : The nuclear magnetic resonance spectra were recorded in a Bruker AVANCE^{II} 300 and Bruker Avance DRX 300

LDI-TOF : Mass spectroscopy performed with an Ultraflex (TOF/TOF) spectrometer.

FT-IR measurements : All FTIR measurements were recorded in Perkin Elmer (Spectrum one). The samples were of solid porphyrins (recovered after evaporation of solvent in a non-controlled precipitated way) and were performed in attenuated total reflection (ATR) mode. Porphyrins were measured on the plate of universal ATR (UATR).

CD measurements : A Jasco J-275 spectropolarimeter was used for CD spectra measurements. A Peltier-temperature programmer for thermosettting the samples was used to cool the solutions. The samples were transferred to a quartz cuvette to be analyzed. When the measured temperature was reached and stabilized, spectra were recorded.

UV-Visible absorption measurements : UV-Visible absorption measurements were performed using a UV-Vis-NIR Varian, model Cary 5000 instrument using 1 cm length quartz cell. All the samples were prepared, diluting a solid sample of the porphyrin and BCP in the corresponding amount of solvent.

Fluorescence spectroscopy measurements : The fluorescence measurements were performed using a Horiba-Jobin-Yvon SPEX Nanolog-TM and Cary eclipse spectrofluorimeters. All the samples were prepared, diluting a solid sample of the porphyrin and BCP in the corresponding amount of solvent.

4.7.1. N-Octadecyl-2-chloroacetamide 4

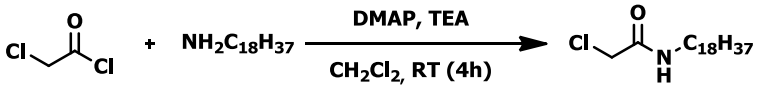

4

Chloroacetyl chloride (2.5 ml, 31.4 mmol) and N-N-dimethyl-4-aminopyridine (0.125 mg) were dissolved in dichloromethane (62 ml). This solution was cooled to 0 ºC and octadecylamine (10.13 g, 37.7 mmol) with triethylamine (10.5 ml, 75.4 mmol) in dichloromethane (15 ml) was added dropwise over one hour. The resulting solution was stirred for a further three hours at room temperature. The solvent residue was filtered and the filtrate was treated with HCl (1 M) by extraction. The resulting organic phase was dried using $MgSO_4$ anhydrous. Finally, the organic solvent was filtered and evaporated to give 7.0 g of a white solid (64.4 %). **M.F. :** $C_{20}H_{40}ClNO$; **M.W. :** 345.99 g/mol ; **^{1}H NMR** (250 MHz, *d*-Chloroform) δ 6.57 (s, 1H; NH), 4.04 (s, 2H; $ClCH_2CONH$), 3.32-3.27 (m, 2H; $CONHCH_2(CH_2)_{16}CH_3$), 1.5-1.2 (m, 32H; $CONHCH_2(CH_2)_{16}CH_3$), 0.88 (t, J=6.2 Hz, 3H; $CONHCH_2(CH_2)_{16}CH_3$) ; **IR-ATR** (cm^{-1}) : 3292 (m, NH), 2954 (s, CH_2), 2916 (s, CH_2), 2848 (s), 1666 (s, CONH), 1645 (s, CONH), 1551 (m, CONH), 1468 (m), 1415 (w), 1375 (w), 1301 (w), 1264 (w, C-N), 1233 (w), 1161 (w), 720 (w, N-H).

4.7.2. 2-(4-Formylphenoxy)-N-octadecylacetamide 5

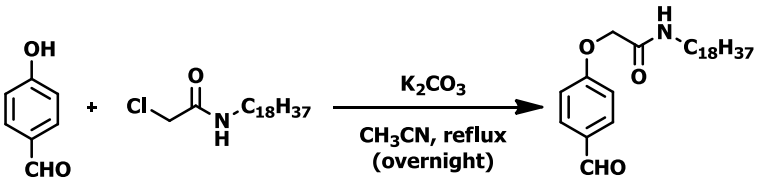

4 5

4-Hydroxybenzaldehyde (1.48 g, 12.14 mmol) and N-octadecyl-2-chloroacetamide (3.5 g, 10.1 mmol) were dissolved in dry acetonitrile (180 ml) and dry potassium carbonate (7.0 g, 50.55 mmol) was added. The mixture was refluxed overnight under inert atmosphere. The cool solution was filtered and the solid residue was washed with acetonitrile, and then dissolved in CH_2CH_2/EtOAc (1:1) (60 ml), filtered and the solvent evaporated leaving a brownish powder (2.70 g, 61.8 %). **M.F. :** $C_{27}H_{45}NO_3$; **M.W. :** 431.65 g/mol ; **^{1}H NMR** (250 MHz, *d*-Chloroform): δ 9.92 (s, 1H, CHO), 7.88 (d, J=8.7 Hz, 2H; ArH), 7.05 (d, J=8.7 Hz, 2H; ArH), 6.49 (s, 1H, CONH), 4.57 (s, 2H; OCH_2CONH), 3.35 (m, 2H; $CONHCH_2(CH_2)_{16}CH_3$), 1.56 (m, 2H; CONH $CH_2CH_2(CH_2)_{15}CH_3$), 1.24-1.21 (m, 32H; $CONHCH_2(CH_2)_{16}CH_3$), 0.89 (t, J=6.0, 3H; $CONHCH_2(CH_2)_{16}CH_3$).

4.7.3. Synthesis of the achiral porphyrin 2

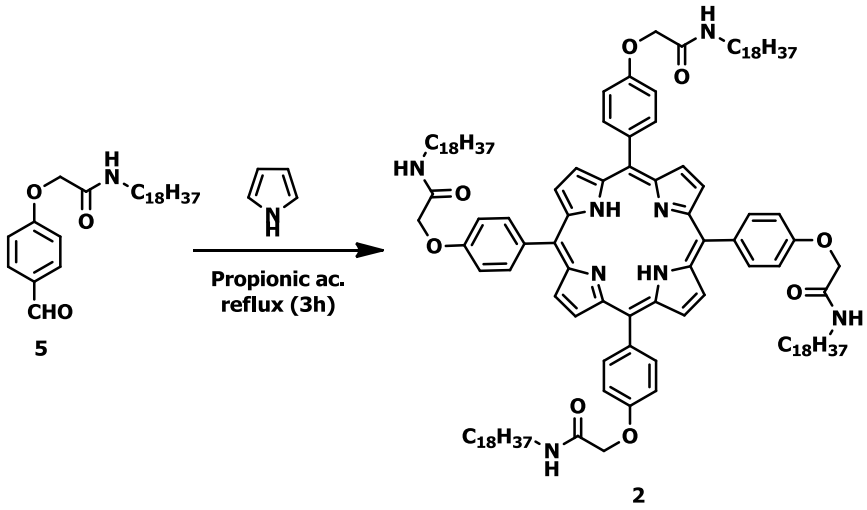

The achiral aldehyde derivative **5** (400 mg, 0.93 mmol) was dissolved in propionic acid (10.0 ml) and the solution was refluxed with vigorous stirring for 30 minutes in air. Pyrrole (64.2 µl, 0.93 mmol) freshly filtered through neutral alumina was added drop by drop at 150 ºC and then the mixture was allowed to reflux for about 3 hours. Propionic acid was distilled under reduced pressure. The dark crude product was subjected to column chromatography on silica gel for purification (Toluene/EtOAc, 8:2) and the desired achiral porphyrin **2** was obtain as a purple solid (140 mg, 7.9 %).

4.7.4. Synthesis of (R)-Methyl 2-(4-formylphenoxy)propanoate (R)-6

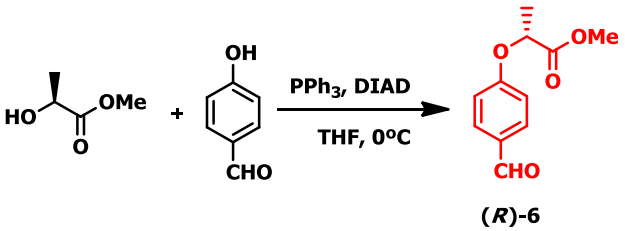

4-hydroxy-benzaldehyde **1** (10.0 g, 81.9 mmol), *S*-(-)-methyl lactate **2** (9.40 ml, 98.3 mmol) and triphenylphosphine (25.8 g, 98.3 mmol) were dissolved in anhydrous THF (300 ml). The mixture was stirred vigorously at 0 ºC and under Ar atmosphere for 10 minutes. A second solution of diisopropyl azodicarboxylate (19.4 ml, 98.3 mmol) in anhydrous THF (100 ml) was added dropwise over 30 minutes. The resulting solution was stirred overnight at room temperature. H_2O was added in order to quench the reaction and then the solvent was removed under pressure. The aqueous solution was extracted with CH_2Cl_2 (3x20 ml) and the organic phase was dried over

$MgSO_4$ anhydrous. Finally, the organic solvent was filtered through cotton wool and evaporated to give yellow oil. The crude compound was purified by silica gel column chromatography (hexane/EtOAc, 8:2) to obtain 14.2 g (83.1 %) of the desired compound (*R*)-**6**. **M.F. :** $C_{11}H_{12}O_4$; **M.W. :** 208.22 g/mol: **^{1}H-NMR** (250 MHz, *d*-chloroform) δ 9.80 (s, 1H; CHO), 7.74 (d, *J* = 8.6 Hz, 2H; ArH), 6.90 (d, *J* = 8.8 Hz, 2H; ArH), 4.82 (q, *J* = 6.8 Hz, 1H; OCH(CH_3)), 3.69 (s, 3H; $COOCH_3$), 1.59 (d, *J* = 6.8 Hz, 3H; OCH(CH_3)) : **$[\alpha]_{546literature}$ =** +46 deg·cm^2/mg **$[\alpha]_{546observed}$ =** +43 deg·cm^2/mg (c=0.19 M; CH_2Cl_2).

4.7.5. Synthesis of the chiral lactate porphyrin (*R,R,R,R*)-3

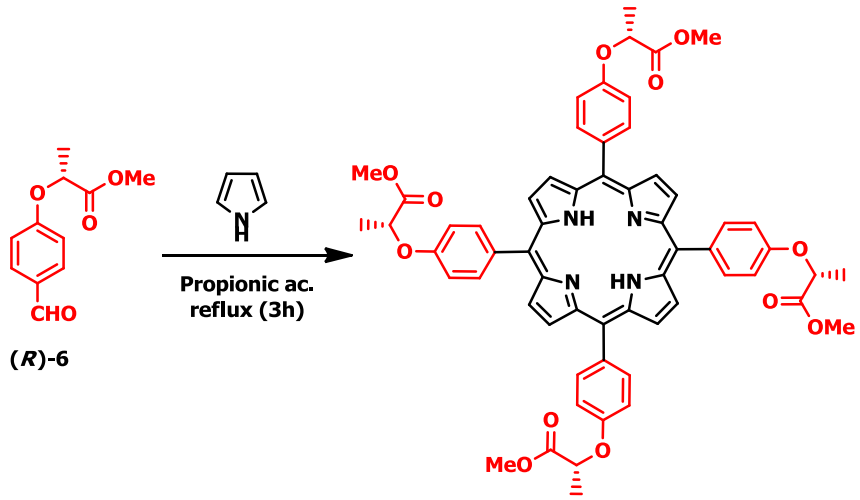

(*R*)-6

(*R,R,R,R*)-3

The lactate aldehyde derivative (2.5 g, 12.0 mmol) was dissolved in propionic acid (45.0 ml) and the solution was refluxed with vigorous stirring for 30 minutes in air. Pyrrole (0.83 ml, 12.0 mmol) freshly filtered through neutral alumina was added drop by drop at 150 ºC and then the mixture was allowed to reflux for about 3 hours. Propionic acid was distilled under reduced pressure. The dark crude product was subjected to column chromatography on silica gel for purification (CH_2CH_2/1 % MeOH) and 0.7 g (5.7 %) of the desired chiral lactate porphyrin (*R,R,R,R*)-**3** was obtain as a purple solid. **M.F. :** $C_{60}H_{54}N_4O_{12}$; **M.W. :** 1022.88 g/mol ; **^{1}H-NMR** (250 MHz, *d*-chloroform) δ 8.89 (s, 8H; pyrrole), 8.14 (d, *J* = 8.5 Hz, 8H; ArH), 7.28 (d, *J* = 8.5 Hz, 8H; ArH), 5.10 (q, *J* = 6.7 Hz, 4H; OCH(CH_3)), 3.94 (s, 12H; $COOCH_3$), 1.85 (d, *J* = 6.8 Hz, 12H; OCH(CH_3)), -2.72 (s, 1H; NH) ; **FT-IR (KBr)** (cm^{-1}) : 2992 (w, CH_3), 2949 (w, CH_3), 1756 (s, $COOCH_3$), 1736 (s, $COOCH_3$), 1597 (m, phenyl), 1506 (m, phenyl), 1471 (m), 1282 (m), 1204 (s), 1177 (m), 1133 (s, OCH_3), 1098 (m), 806 (m).

4.7.6. Synthesis of the desired chiral porphyrin (*R,R,R,R*)-1

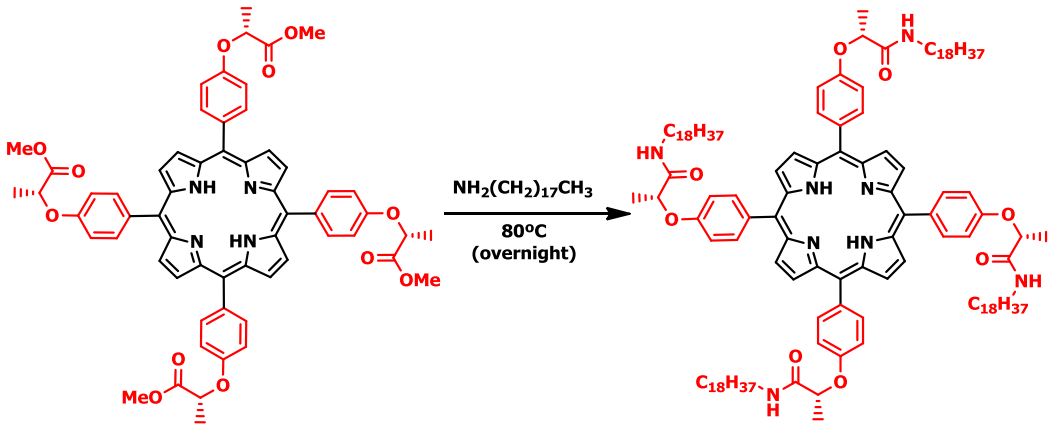

(*R,R,R,R*)-3 (*R,R,R,R*)-1

The lactate porphyrin (*R,R,R,R*)-**3** (700 mg, 0.68 mmol) and an excess of octadecylamine (1.50 g, 5.44 mmol) were mixed and heat at 80 ºC overnight. The mixture was cooled down to room temperature to obtain a dark red crude compound. The product was purified by a silica gel chromatography and exclusion chromatography to the complete removal of the octadecylamine to afford 1.02 g (75.7 %) of the desired porphyrin as a purple solid. **M.F. :** $C_{128}H_{194}N_8O_8$; **M.W. :** 1972.96 g/mol ; ^{1}H NMR (360 MHz, *d*-chloroform) δ 8.83 (s, 8H; pyrrole), 8.13 (d, *J* = 8.5 Hz, 8H; ArH), 7.27 (d, *J* = 8.4 Hz, 8H; ArH), 6.68 (t, *J* = 6.0 Hz, 4H; CONH), 5.00 (q, *J* = 6.8 Hz, 4H; OCH(CH_3)), 3.41 (m, 8H; CONHCH_2(CH_2)$_{16}$$CH_3$), 1.80 (d, *J* = 6.7 Hz, 12H; OCH(CH_3)), 1.60 (m, 8H; CONHCH$_2$$CH_2$($CH_2$)$_{15}$$CH_3$), 1.20 (m, 120H; CONHCH$_2CH_2$($CH_2$)$_{15}$$CH_3$), 0.85 (t, *J* = 6.9 Hz, 12H; CONHCH$_2$(CH_2)$_{16}$$CH_3$), -2.79 (s, 2H; NH) ; **FT-IR (KBr)** (cm^{-1}) : 3286 (w, NH), 2924 (s, CH_2), 2852 (s, CH_2), 1657 (s, CONH), 1606 (m, phenyl), 1497 (m, phenyl), 1466 (s), 1277 (w), 1235 (m), 1176 (m), 1085 (w), 800 (m).

4.7.7. General procedure for metallation

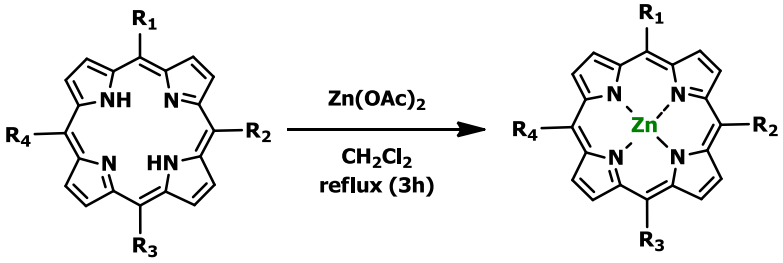

In separate reactions, each porphyrin (*R,R,R,R*)-**3** (150 mg, 0.15 mmol), (*R,R,R,R*)-**1** (360 mg, 0.17 mmol) and **2** (140 mg, 0.073 mmol)) were dissolved in CH_2Cl_2 ($7.5\cdot10^{-3}$ M) under stirring and argon atmosphere. Zinc acetate dissolved in 1:1 mixture of CH_2Cl_2/MeOH (0.052 M) was added

drop wise with syringe over 5 minutes. The reaction mixture was refluxed further three hours. Dichloromethane was added and the organic layer was washed with a saturated aqueous solution of sodium bicarbonate, brine and was dried over anhydrous Na_2SO_4 and concentrated *in vacuum*. The residue was purified by silica gel chromatography (CH_2Cl_2/1.5 % MeOH) giving the desired metalloporphyrins as a purple metallic powder.

[5,10,15,20-[4-(*R,R,R,R*)-methyl 2-phenoxy propanoate] porphyrin] zinc (II), Zn-(*R,R,R,R*)-3. M.F. : $C_{60}H_{52}N_4O_{12}Zn$; **M.W. :** 1086.45 g/mol ; **^{1}H-NMR** (300 MHz, acetone-d_6) δ 8.88 (s, 8H; pyrrole), 8.11 (d, J = 8.2 Hz, 8H; ArH), 7.31 (d, J = 8.6 Hz, 8H; ArH), 5.24 (m, 4H; O<u>CH</u>(CH_3)), 3.87 (s, 12H; $COOCH_3$), 2.78 (d, J = 9.6 Hz, 12H; OCH(<u>CH_3</u>)) ; **IR-ATR** (cm^{-1}) : 2992 (w, CH_3), 2949 (w, CH_3), 1751 (s, $COOCH_3$), 1741 (s, $COOCH_3$), 1598 (m, phenyl), 1556 (w, phenyl), 1506 (m, phenyl), 1503 (w, phenyl), 1234 (s) ; **UV-Vis** (CH_2Cl_2) λ_{max}/nm (ε M^{-1} cm^{-1}) : 422 (521900), 550 (21962), 590 (6230) ; **UV-Vis** (CH_2Cl_2) λ_{max}/nm (ε M^{-1} cm^{-1}) : 422 (521900), 550 (21962), 590 (6230).

[5,10,15,20-[4-(*R,R,R,R*)-2-*N*-octadecylamidoethyloxiphenyl] porphyrin] zinc (II), Zn-(*R,R,R,R*)-1. M.F. : $C_{128}H_{192}N_8O_8Zn$; **M.W. :** 2036.32 g/mol ; **Found LDI-Tof [M^+] :** 2034 ; **^{1}H-NMR** (300 MHz, *d*-chloroform) δ 8.91 (s, 8H; pyrrole), 8.12 (d, J = 8.4 Hz, 8H; ArH), 7.10 (d, J = 8.5 Hz, 8H; ArH), 6.46 (t, J = 5.8 Hz, 4H; CONH), 4.28 (m, 4H; O<u>CH</u>(CH_3)), 3.00 (q, J = 6.4 Hz, 8H; CONH<u>CH_2</u>(CH_2)$_{16}$$CH_3$), 1.38 (d, J = 6.6 Hz, 12H; OCH(<u>CH_3</u>)), 1.22 (m, 128H; CONHCH$_2$(<u>CH_2</u>)$_{16}$$CH_3$), 0.86 (t, J = 6.8 Hz, 12H; CONHCH$_2$(CH_2)$_{16}$<u>CH_3</u>) ; **IR-ATR** (cm^{-1}) 3322 (w, NH), 2921 (s, CH_2), 2852 (s, CH_2), 1650 (w, CONH), 1505 (w, phenyl), 1234 (s) ; **UV-Vis** ($CHCl_3$) λ_{max}/nm (ε M^{-1} cm^{-1}) : 426 (34493), 555 (16809), 597 (6854).

[5,10,15,20-[4-*N*-octadecylacetamidophenoxy] porphyrin] zinc (II), Zn-2. M.F. : $C_{124}H_{184}N_8O_8Zn$; **M.W. :** 1980.22 g/mol : **^{1}H NMR** (300 MHz, *d*-chloroform) δ 8.93 (s, 8H; pyrrole), 8.16 (d, J = 8.6 Hz, 8H; ArH), 7.29 (d, J = 8.7 Hz, 8H; ArH), 6.77 (m, 4H; CONH), 5.30 (s, 8H; O<u>CH_2</u>CONH), 3.22 (m, 8H; CONH<u>CH_2</u>(CH_2)$_{16}$$CH_3$), 1.23 (m, 128H; CONHCH$_2$(<u>$CH_2$</u>)$_{16}$$CH_3$), 0.86 (m, 12H; CONHCH$_2$($CH_2$)$_{16}$<u>$CH_3$</u>) ; **IR-ATR** ($cm^{-1}$) : 3321 (s, NH), 2917 (s, CH_2), 2851 (s, CH_2), 1655 (s, CONH), 1607 (m, phenyl), 1536 (s), 1504 (m, phenyl), 1468 (m), 1282 (m), 1235 (s), 1175 (m), 1056 (m), 801 (m) ; **UV-Vis** ($CHCl_3$) λ_{max}/nm (ε M^{-1} cm^{-1}) : 424 (86634), 556 (5882), 598 (2531).

5. Summary

This thesis has focused in the synthesis of different chiral porphyrins in which the phenyl lactate derivative gives the stereogenic center to the system. Moreover, the self-assembly of these chiral chromophores by different non-covalent interactions such as hydrogen-bonding, π-π stacking or metal coordination and the influence of them in the supramolecular organization of organic molecules has been studied in solution and in the solid state.

Chapter 2 **: Self-assembly of chiral porphyrins and metalloporphyrins through coordination and hydrogen bonds ;** It has been shown that a family of free-base porphyrins and metalloporphyrins which contain chiral amide groups and pyridyl groups as a substituent in the *meso*-position showed different self-assembly depending on the constitution of the chromophirc ring. The free-base porphyrins do not show self-assembly in solution, whereas the chiral zinc (II) metalloporphyrins of the same family can exhibit hierarchical self-assembly driven by the zinc (II) interaction with pyridyl moieties as the dominant interaction, but hydrogen-bonding and van der Waals interactions are responsible for the massive increase in optical activity that is observed. Moreover, the deposition of metalloporphyrin aggregates onto graphite reflects the state of assembly in solution. Furthermore, the morphology of the aggregates formed out-of equilibrium conditions on solid state enhances weak interactions in their assembly.

Chapter 3 **: Bottom-up approach to C3 symmetric chiral aggregates ;** It has been shown that a chiral C_3 discotic molecule self-assembles in different solvents through π-π interactions between the porphyrin rings. The more extended π system and planar conformations of these units, engage more efficiently in π-π interactions than the π–stacking among benzene-tris(bipy) core. Moreover, the solvent and the nature of the surface influence in the hierarchy organization of the aggregates upon deposition.

Chapter 4 **: Formation of chiral metalloporphyrin-block copolymer complex through metal coordination ;** The titration studies of the an achiral zinc(II) porphyrin and its homologous chiral metalloporphyrin demonstrate the formation of a complex with a block copolymer through the coordination of the pyridyl unit of one block with the zinc (II) metal ion in the core of the porphyrin ring. Furthermore, the CD studies of the chiral complex showed chirality transfer from the metalloporphyrin monomer to the superstructure of the supramolecular polymer.